
Global- and Ocean-scale Primary Production from Satellite Observations

Author: David Antoine

4.1 INTRODUCTION

4.1.1 Overview of the Chapter Content and Changes from the Previous Editions of the Manual

The launch of the Coastal Zone Color Scanner (CZCS) aboard the NASA *Nimbus-7* satellite in November 1978 (Hovis et al. 1980; Gordon et al. 1980) provided a totally new and unexpected picture of the distribution of the algal biomass, from local (bays, coastal areas, etc.) to global scales. The revealed complexity and variability revolutionized the way phytoplankton dynamics was considered. About fifteen years were then necessary before the first estimates of the global oceanic primary production, as derived from the compilation of the complete CZCS observations, were published (Longhurst et al. 1995; Antoine et al. 1996; Behrenfeld and Falkowski 1997b). This time lag was actually needed to develop or adapt the tools and models necessary to transform global maps of phytoplankton biomass, which provide information about a stock of carbon, into maps of the flux of carbon going through this biomass, i.e., the so-called primary production.

This chapter summarizes important aspects and difficulties of this transformation when performed using remote-sensing information to cover a regional to global scale. It is not, however, a historical review of all the work that has been performed along this line, which would obviously be much longer than the present text. New techniques also have emerged, using other satellite-derived information such as altimetry, in order to indirectly estimate the ocean productivity; these are only mentioned in this chapter.

We first define photosynthesis, primary production, and the significance of this flux in the global carbon cycle. This cycle is presently in a non-steady state and its evolution is uncertain (e.g., Falkowski et al. 1998). Section 4.2 gives a rapid review of the parameters accessible from space and relevant to the modeling of primary production. A rather detailed section about ocean color remote sensing is then provided in Section 4.3. The rationale for this detail is, on the one hand, that ocean color is one of the main observations used in modeling primary production from space and one of its most obvious signatures, and, on

the other hand, that this important field of remote sensing is not covered elsewhere in this manual. Section 4.4 covers the modeling itself, while Section 4.5 describes the global distribution of quantities that directly enter into this modeling or that determine some of its parameters. Section 4.6 summarizes some recent works that present global determinations of oceanic primary production using satellite observations.

If we refer to the two former editions of the *Manual of Remote Sensing*, we find two paragraphs on “chlorophyll detection” in the first edition (1975), which introduced the basic principle of ocean color remote sensing, i.e., the differential absorption of phytoplankton in the blue and green parts of the electromagnetic spectrum. Reference was made mostly to the seminal work of Clarke and co-workers (e.g., Clarke et al. 1970). No ocean color satellite instruments existed at that time.

The second edition appeared eight years later (1983), more than twenty years ago, when ocean color science was still in its infancy. The Coastal Zone Color Scanner (CZCS) had provided observations for only about three years, and most work was on algorithm development and deriving geophysical properties of interest from this new source of data. Biological oceanography was about 24 pages of the 125 pages devoted to the “marine environment” (Chapter 28 at that time), of which only about seven pages dealt with passive detection of oceanic chlorophyll from ocean color.

Clearly, at that time ocean color was not considered a tool of prime interest, since its benefits for oceanography in general, not only for biological oceanography, had not been fully realized. The situation is now profoundly modified, with several new-generation sensors in orbit. Thousands of scientists and other users work with the data, and ocean color is considered with the same interest that thermal infrared remote sensing or altimetry was considered ten or fifteen years ago, namely, as one of the key parameters needed to monitor and understand changes in our oceanic environment.

4.1.2 Photosynthesis and Primary Production

Extensive literature exists on photosynthesis and primary production (e.g., Rabinowitch and Govindjee 1969; Falkowski and Woodhead 1992; Falkowski and Raven 1997; Geider and MacIntyre 2002). We concentrate here on the problem of estimating this production from space observations, in particular from ocean color.

In oceanic waters, the so-called primary production characterizes the capacity of the illuminated portion of the water column to synthesize organic molecules, starting with simple carbohydrates, through the process of photosynthesis. This productivity, which is carried out by the unicellular algae collectively called phytoplankton, is usually expressed in terms of a mass of carbon fixed per unit volume and time (units of a flux: $\text{gC m}^{-3} \text{ s}^{-1}$), and the primary production is the quantity of carbon resulting from the integration of this flux over a certain time and area, and is usually expressed as gC m^{-2} for the duration in question (the day, for instance). Production occurs in the lit portion of the water column, i.e., depths less than 200 m. In summary, photosynthesis is the process involved, primary production is the quantity of carbon fixed through this process, and the productivity could be defined as the efficiency of the overall operation. This last term is used misleadingly, with varying acceptance in the literature, so we will not use it here.

Marine photosynthesis (see Figure 4-1) is often described as a two-step process (each “step” being subdivided into a myriad of different reactions), because one of the steps is light-dependent, while the other is not. In the former, photons are absorbed by chlorophyll and accessory pigments in such a way that electrons are excited to higher energy states. In a series of reactions, referred to as the electron transport process, this energy is converted

into ATP (adenosine triphosphate) and NADPH (nicotinamide adenine dinucleotide phosphate). This is done in the so-called “photosystems,” which are complexes of chlorophyll and other pigment molecules and proteins. At the same time water is split, releasing oxygen as a byproduct of photosynthesis. This makes photosynthesis of geological interest, since it has progressively changed the Earth’s atmosphere to its present composition. Photosynthesis also modulates the oxidation state of the ocean, which in turn can determine the supply of trace elements such as iron (Falkowski et al. 1998).

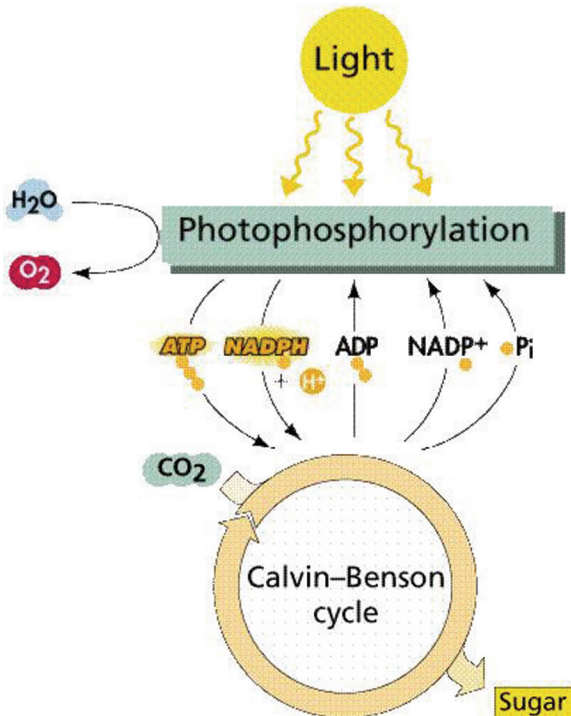


Figure 4-1 Overview of the two steps in the photosynthesis process. Source: Purves et al. 2003.

The energy stored in ATP and NADPH is then used in the second, light-independent, step of photosynthesis, to produce carbon-to-carbon bonds, which are necessary to generate carbohydrates, i.e., the first and basic organic compounds that will be used in subsequent reactions in cells. The “CO₂ to sugar” conversion is known to occur in the “Calvin-Benson” cycle (see also Figure 4-1), which is regulated by a series of enzymatically controlled reactions.

In summary, light is absorbed by pigments (among which is the ubiquitous chlorophyll-a molecule) in order to make energy usable. Enzymes also come into play, their efficiency being temperature-dependent, and their composition requiring some oligo-elements such as iron. Remote-sensing techniques will be of interest for modeling primary production to the extent that they can provide, more or less directly, information about these basic determinants.

Even though photosynthesis is a relatively well-defined process (but see Behrenfeld et al. 2004), the operational definition of “primary production” can vary significantly. A first dichotomy derives from the source of nutrients that fuel production. Either they are newly brought into the upper well-lit layers of the ocean (upwelling, eddy diffusivity, etc.) and the production is then referred to as the “new production,” or they are locally produced in the photic zone through recycling of organic matter and the production is referred to as “regen-

erated production" (Dugdale and Goering 1967). One point of interest in these definitions lies in the equality between the new production and the export of organic matter from the upper layers to the ocean interior, when the processes are considered over sufficiently long time-scales (Eppley and Peterson 1979). The physical mechanisms behind these equations make new production and export of organic matter accessible to satellite remote sensing (see Section 4.4.3).

Other adjectives or prefixes can be appended to production that have more to do with the different ways of measuring it at sea and with the time scale of these measurements. A lot can be read about these aspects (e.g., Williams 1993) that is less relevant to our subject. Some additional insight will be provided in Section 4.4.3.

4.1.3 Significance of Primary Production in the Global Carbon Cycle

A recurrent issue in oceanography and geochemistry concerns the behavior of the global carbon cycle (Figure 4-2) in response to the man-induced increase in the atmospheric carbon dioxide (CO_2) concentration. Is it conceivable that this excess of CO_2 is eventually absorbed by the oceanic or terrestrial biospheres? Alternatively, this increase in CO_2 may intensify the natural greenhouse effect in such a way that the mean temperature of the globe will still rise significantly (IPCC 2001; Hansen et al. 1999). Recently, the effect of atmospheric aerosols (anthropogenic or natural) has also been stressed, with a possible counter-effect, i.e., cooling of the atmosphere, due to an increase of the amount of radiation backscattered toward space (e.g., Andreae 1996). When the sources of CO_2 to the atmosphere (burning of fossil fuels and land use changes), the net CO_2 increase in the atmosphere, and the oceanic CO_2 sink are summed, it is found that the budget is not balanced. A "missing sink" appears. This probably does not mean that some unknown process occurs somewhere on the planet, but rather that a larger than expected uncertainty exists on one or more of the carbon fluxes presently identified when assessing the carbon budgets. It could be that the ocean contributes to this sink. Therefore, increasing our capability in modeling and predicting the oceanic primary production, as well as the fate of the carbon produced through this process, is a key for the better understanding of the global carbon cycle.

To make this prediction we must first evaluate the nature and size of the carbon pools (ocean, atmosphere, terrestrial biosphere, carbonaceous sediments, soils) and the fluxes between them. The processes governing these fluxes must be identified and understood. These topics are usually referred to as "global change" studies.

The oceanic phytosphere, commonly indexed through the phytoplankton pigment content (usually the chlorophyll concentration), is one of the crucial carbon pools to be considered. The carbon reservoir is small when compared to terrestrial plants (less than 1/500), yet it is responsible for one of the largest carbon fluxes on Earth, namely the oceanic primary production that amounts to about 50 Giga tons of carbon per year (Longhurst et al. 1995; Antoine et al. 1996; Behrenfeld and Falkowski 1997b). This is due to the high turnover rate of carbon in the oceanic autotrophic biomass, which is approximately one week. World annual photosynthetic carbon fixation is nearly-equally shared between land and ocean (e.g., Field et al. 1998). However, only a fraction of the organic carbon generated through the photosynthetic process is exported from the upper oceanic layers towards the ocean floor (the "export production"). This mechanism of transfer is referred to as the oceanic "biological pump." This pump results in sequestering atmospheric CO_2 into deep-sea sediments. This fraction of the total flux is small (probably less than 5%) (Honjo 1980; Deuser and Ross 1980), yet highly significant from a geological point of view, since over time a huge carbon reservoir builds up in sedimentary carbonate rocks.

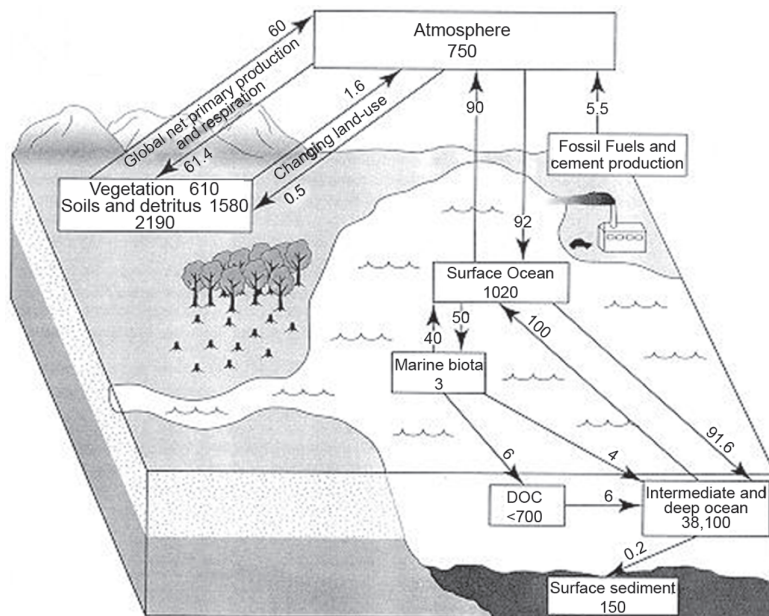


Figure 4-2 The global carbon cycle. Carbon “reservoirs” (where carbon is stored) are represented by boxes, and the units are the gigatons of carbon contained in each reservoir. Carbon “fluxes” (transfers of carbon between reservoirs) are represented by arrows, and their units are gigatons of carbon per year. A gigaton is the same quantity as a petagram, which is 10^{15} grams. Source: Schimel et al. 1995. Reprinted with the permission of Cambridge University Press.

The relevance to global change issues of studying the marine biosphere and its renewal rate lies in the possible changes, over decades, perhaps less, of the strength of the “biological pump,” with the corresponding effect on atmospheric CO₂. Such changes have been identified for the last interglacial-glacial transition. Predicting, or at least identifying, these changes is critical for long-term policies about CO₂ emissions. Identification of changes in the strength of this pump is probably not sufficient, since we also need to understand the pump’s structure and functioning. Which is the limiting nutrient? What are the species assemblages? The latter is probably more important in defining the capacity of the ocean to sequester atmospheric CO₂. Remote sensing is again of some help in these qualitative assessments, for instance through the use of multispectral (even hyperspectral) systems that could help in discriminating functional groups of phytoplankton.

Ocean color remote sensing allows the phytoplankton pigment content of the upper ocean to be monitored. This piece of information, with the repetitive coverage of large portions of the Earth gained from remote sensing, forms one piece in the overall strategy of global change research. The principle was built in the 1970s (Clarke et al. 1970), and the first experimental instrument was the Coastal Zone Color Scanner (CZCS), launched on the NASA *Nimbus-7* satellite (Hovis et al. 1980; Gordon et al. 1980). Several new-generation instruments have been launched since the CZCS died, such as the Japanese OCTS (Saitoh 1995) and the French POLDER (Deschamps et al. 1994) in August 1996, both unfortunately lost in June 1997; the US SeaWiFS in August 1997 (Hooker et al. 1992), now operating; the US MODIS instruments (Salomonson et al. 1989) in December 1999 and May 2002; and the European MERIS aboard the Envisat platform in March 2002 (Rast and Bézy 1995). The purpose of these instruments is to provide users with several types of data, on a global and repetitive basis, precisely to address global change issues.

4.2 WHAT DO WE SENSE FROM SPACE THAT IS USEFUL FOR THE MODELING OF OCEANIC PRIMARY PRODUCTION?

To answer this question, we must identify the parameters relevant to oceanic primary production and the techniques that can be applied from space to provide information at the necessary accuracy and with the correct time and space scales.

Primary production is the quantity of carbon fixed through photosynthesis, a process that always goes through a chlorophyll molecule. Ocean color (Section 4.3) is the relevant technique to determine the quantity of chlorophyll per unit volume within the upper layers of the ocean. The extent to which surface information is useful to estimate a depth-integrated quantity is examined in Section 4.4.1.

Chlorophyll captures photons, some of which are brought by other pigments that only serve as photon carriers. The energy of these photons permits transfer of electrons within the “reaction center,” which is a complex of chlorophyll molecules and proteins. An extremely complex chain of reactions then reduces the carbon dioxide to carbohydrates. Light is therefore the other quantity (or flux) that we have to consider. By light, we mean the number of photons and their spectral energy distribution, which is multiplied by the absorption spectrum of phytoplankton to determine the amount of absorbed energy. Any sensor in orbit that records the radiance within the visible part of the electromagnetic spectrum can provide information about the light backscattered to space and therefore, from indirect estimation, about the light reaching the ocean surface. This is one way to measure the spectrum of the incoming photon flux.

Models also exist that allow the clear-sky irradiation at the sea surface to be computed quite accurately, solely from knowledge of the date and the latitude, and using some mean values for absorption by ozone, and scattering and absorption by aerosols (e.g., Gregg and Carder 1990). By using appropriate parameterizations, the clear-sky values can be corrected for the effect of clouds in order to provide the actual irradiation reaching the surface (e.g., Reed 1977). Therefore, simple information about cloudiness (meteorological sensors) may also suffice to get the relevant information about irradiation (Rossow and Schiffer 1991).

Recently these two approaches were pooled together using detailed modeling of radiation interaction with clouds (Frouin et al. 2003) in order to provide the daily irradiation at the sea surface at the same resolution as the satellite data, using the actual cloudiness provided as a byproduct of the ocean color observations.

A second-order effect of light (UV radiation) is to damage the photosynthetic apparatus of phytoplankton (e.g., Helbling et al. 1992; Smith et al. 1992). Quantifying this effect may also require an accurate determination of the incoming flux in this spectral domain, the present sensors not being equipped with the relevant spectral bands.

To complete the picture, ozone mapping systems (McPeters et al. 1996) are also of interest when trying to model the irradiation at the sea surface by providing the amount of ozone absorption in the Chappuis band (centered around 600 nm).

Having determined the amount and spectral composition of light at the surface, it remains to propagate this energy into the water column. Again phytoplankton comes into play. To this extent, no additional measurement is needed to complement ocean color, at least if the absorption spectrum of phytoplankton is known. In Case 2 waters (Section 4.3.2.1), other substances such as sediments and dissolved organic compounds affect the irradiance propagation. In principle these are also derivable from the ocean color spectrum (e.g., Moore et al. 1999).

The energy of photon absorption is progressively transferred through a chain of reactions, which, at a certain point, are enzymatically controlled. This is the “dark part” of primary production that is independent of the light level. As a consequence, the ambient temperature is also a parameter to consider. This is also measurable from space using thermal infrared radiometers. Satellite sea surface temperature (SST) concerns the very surface (a few microns), while the relevant information for photosynthesis is the vertical profile of temperature or at least a reasonable estimate of the mean value within the euphotic layer, i.e., the depth where irradiance is reduced to 1% of its value just below the surface. More than 90% of primary production takes place within this layer. Inferring the vertical temperature profile or the mean temperature within the euphotic layer, along with the vertical distribution of phytoplankton, is discussed in Section 4.4.1.

From H_2O and CO_2 , simple carbohydrates can be produced. For cell growth (e.g., synthesis of proteins and nucleic acids) other elements are necessary, primarily nitrogen and phosphorus, but also less abundant elements such as iron, silica, and other oligo-elements. The situation becomes more complex here because there is no radiometric signature to quantify the concentration of these elements in the surface waters. Only indirect methods are available unless the concentration of some elements can be derived from the concentration of atmospheric aerosols, which can also be assessed from ocean color observations.

For nitrogen, empirical relationships between the SST and the nitrate concentration have been successfully used. Such relationships exist when a strong physical forcing brings deep, nutrient-rich waters to the surface. Because these deep waters are also colder than the surface waters, their nutrient concentrations co-vary with the temperature at the surface. The method is particularly suited for upwelling regions (Dugdale et al. 1989; Sathyendranath et al. 1991), but its relevance vanishes elsewhere.

Another remote sensing technique—radar altimetry—has also provided promising results. One approach with global application is based on relationships between the sea surface height anomaly, the heat storage of the upper ocean, and the nutrient storage. The technique estimates the time rate of change of the nutrient storage. This is related to new production, and then to export of carbon to deep layers. Another technique uses relationships between the sea surface height anomaly and the depth of the $20^{\circ}C$ isotherm, then between this depth and the new production (Turk et al. 2001). The relationships were established from *in situ* data collected in the equatorial Pacific, and therefore cannot be applied outside of this domain.

It must also be mentioned that some of the above observations address not only the reservoirs and fluxes (biomass, irradiation, etc.), but can also be used to determine the values of parameters in models. For instance, temperature modulates the maximum rate of algal photosynthesis, and the mean light level in the upper layer can determine the shape of the photosynthetic curve (see Section 4.4.2).

The suite of remote-sensing techniques that are relevant to modeling oceanic primary production thus includes ocean color (phytoplankton and other optically significant substances, incident radiation, aerosols), thermal infrared radiometry (SST), ozone mapping systems (incident radiation), and altimetry (dynamics of nutrients/mixed-layer). The modeling of oceanic primary production is therefore a topic where the synergistic use of satellite observations from different platforms takes its full meaning.

The following section provides some insight into ocean color and the way geophysical properties of interest for modeling primary production (e.g., chlorophyll) are derived from the spectrum recorded by a satellite-borne sensor.

4.3 OCEAN COLOR AND ITS REMOTE SENSING FROM SPACE

4.3.1 Why Ocean Color is of Interest, in Particular for Modeling Ocean Primary Production

Phytoplankton (Figure 4-3) is the first link of the marine food-web, and its abundance determines the development of higher levels (Figure 4-4). The understanding of marine ecosystems, and the quantification of the exchanges and flows between their various compartments (phytoplankton, zooplankton, detritus, etc.), requires at least a good quantification of the phytoplankton. Moreover, the principal world fishing zones are in areas of strong phytoplankton production, and they should be understood as much as possible.

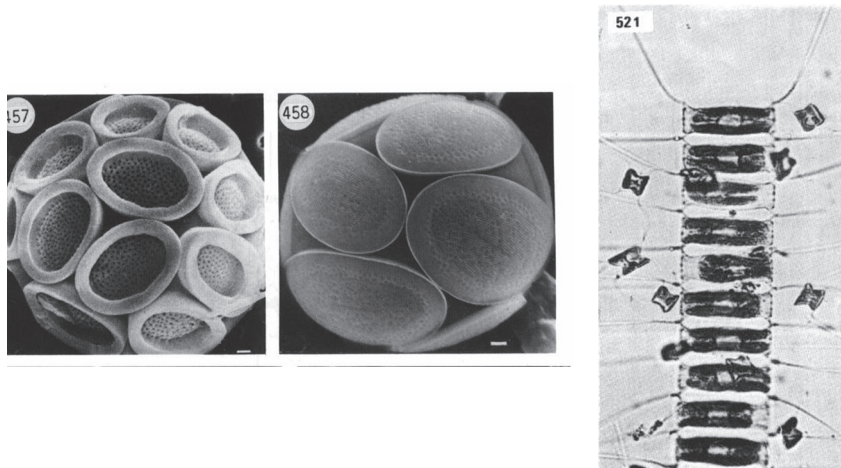


Figure 4-3 Various phytoplanktonic cells. Left: coccolithophorids. Source: Chrétiennot-Dinet 1987; illustrations from *Atlas du Phytoplancton Marin*, Vol. 3 by M. J. Chrétiennot-Dinet, C. Billard, A. Sournia, copyright CNRS EDITIONS, 1987. Right: a diatom. Source: Ricard 1987; illustration from *Atlas du Phytoplancton Marin*, Vol. 2 by Michel Ricard, copyright CNRS EDITIONS, 1987.

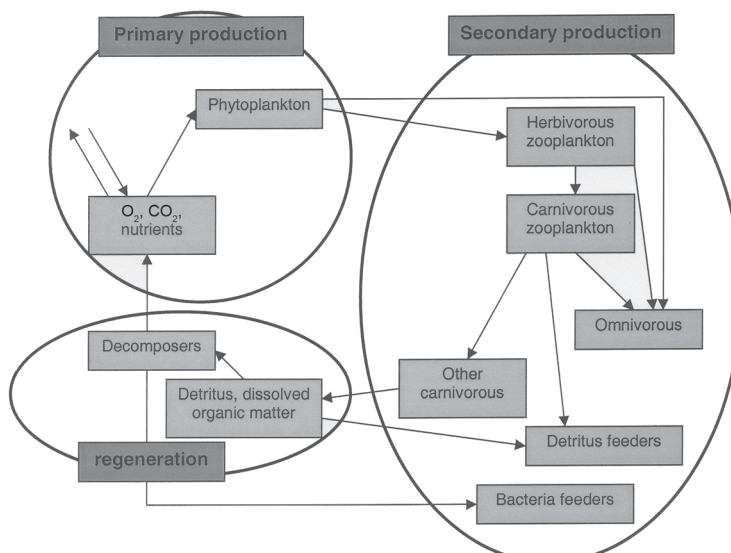


Figure 4-4 Schematic of the food-web in the ocean.

In addition, these photosynthetic algae create organic matter and oxygen by fixing dissolved CO₂ and nutritive elements present in sea water. This matter is partly exported towards the deep layers and ultimately sequestered into the sediments of the oceanic floor. On a sufficiently long time-scale, a net CO₂ flux is created from the atmosphere towards the ocean floor. This process is usually referred to as the “biological pump.” This adds to the more significant “solubility pump,” which describes the transfer of CO₂ due to the changes in its solubility in water of different temperatures. Phytoplankton plays a significant role in the regulation of atmospheric gases and chemical species in the ocean. The knowledge of the global distribution and temporal variations of phytoplankton concentrations is mandatory for a thorough study of global cycles of carbon and associated elements in the ocean.

Lastly, it is of course the synoptic aspect of the satellite observations and their high frequency of acquisition that makes ocean color remote sensing so attractive for the study of the oceanic phenomena, the majority of which are extremely variable in both spatial distribution and temporal evolution. Phytoplankton, as detected from space, is an excellent tracer of these movements, except in the case of a very fast development of the algae population (blooms).

4.3.2 What is “Ocean Color”?

4.3.2.1 REFLECTANCE

Variations of the color of the sea, viewed obliquely from low altitude, from blue in good weather to gray under thick cloud, are due mostly to reflections of light from the sky on the surface of the sea. The “ocean color” that is the focus here will be better observed if one is freed from surface reflections, for instance by measuring beneath the surface of the water. The color will then change from indigo blue, to dark green, and even to brownish. The human eye however has rather specialized spectral response, and the oceanographic parameter “water color” will be more precisely defined as the spectral variations (as a function of wavelength, λ) of the diffuse reflectance of the upper ocean, R(λ) (see Table of Symbols). The reflectance R(λ) is itself the ratio between the irradiance upwelling just under the surface of the water, E_u(λ), to the downwelling irradiance just penetrating the surface, E_d(λ).

Variations of R(λ) are due to the various dissolved substances or suspended particles in water and also to sea water itself. Hence, by methods of inversion, one will be able to obtain information on the properties or the concentrations of these various “additives” to sea water from measurements of R (measured across the visible spectrum, from approximately 400 to 700 nm). This possibility led oceanographers to be interested in “ocean color.”

For the present discussion, we will be interested only in water known as Case 1 (Morel and Prieur 1977), namely open ocean waters, unaffected by river runoff, and more generally, by any influence of the coast or of the bottom. In Case 1 waters (Figure 4-5), which account for approximately 95% of the world’s ocean, the optical properties are determined by sea water itself, and by phytoplankton and all “associated products” (organic refuse in the form of particles or dissolved substances, and heterotrophic organisms). The variations of Case 1 water’s optical properties are in general indexed with respect to the chlorophyll concentration (and not determined solely by the chlorophyll concentration). Chlorophyll is the pigment common to all marine photosynthetic organisms and also the pigment most frequently measured.

All other waters are Case 2, where the optical properties depend on the same components as in Case 1, and also on other optically active substances, like “yellow substances” or suspended materials coming from re-suspension of sediments. The multiple possible combinations between phytoplankton and particles and exogenic dissolved substances (i.e., not

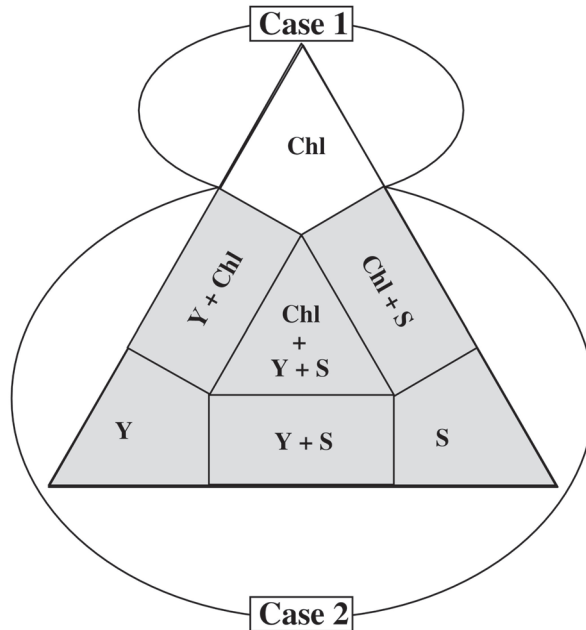


Figure 4-5 Illustration of the various combinations of optically active substances used in determining whether waters are of "Case 1" or "Case 2" ("Chl", "S" and "Y" stand for chlorophyll, sediments, and yellow substances, respectively).

produced by the phytoplanktonic activity) generate a multitude of possibilities for the reflectance spectrum, and its inversion to estimate the concentrations of the various components of this water becomes very difficult. However, due to the economic importance of Case 2 waters, exploring their optical properties and searching for algorithms to invert their reflectance spectra is under active development (IOCCG 2000).

Reflectance can be expressed in terms of the backscattering coefficient, b_b , and the absorption coefficient, a (Morel and Prieur 1977; Gordon 1979)

$$R(\lambda) = F_{L,b} \frac{b_b(\lambda)}{a(\lambda)} \quad (4-1)$$

where $F_{L,b}$ is a proportionality factor, which expresses the fact that R depends on the distribution of underwater radiances, $L(\zeta, \phi)$. F is thus variable with the solar elevation insofar as this changes the radiative field under the oceanic surface, and with the shape of the total volume-scattering function, β . This function changes with the ratio η between molecular scattering and scattering due to the particles (Morel and Gentili 1991).

The inherent optical properties a and b_b can also be broken up into the sum of the coefficients corresponding to the various components (inherent optical properties being additive). For Case 1 waters, these N components are the pure sea water (subscript w), the particles (subscript p), which can be divided into phytoplankton (subscript ϕ), and the other, non-algal particles (subscript nap, in general the difference between p and ϕ), and finally the colored dissolved substances (subscript ds)

$$R(\lambda) = F_{L,\beta} \frac{b_{b,w}(\lambda) + b_{b,p}(\lambda)}{a_w(\lambda) + a_p(\lambda) + a_{ds}(\lambda)} \quad (4-2)$$

with

$$\alpha_p(\lambda) = \alpha_\phi(\lambda) + \alpha_{nap}(\lambda)$$

Finally, the equation above can be expressed by using the corresponding specific coefficients

$$R(\lambda) = F_{L,\beta} \frac{b_{b,w}(\lambda) + \sum_{i=1,N} b^*_b(\lambda)_i [i]}{\alpha_w(\lambda) + \sum_{i=1,N} \alpha^*(\lambda)_i [i]} \quad (4-3)$$

where [i] is the concentration of the i component, and $\alpha^*(\lambda)_i$ and $b^*_b(\lambda)_i$, specific coefficients of absorption and backscattering at the wavelength λ .

Figures 4-6 and 4-7 show how the spectra of $E_d(\lambda)$ and $R(\lambda)$ vary according to the chlorophyll concentration in Case 1 waters. We now examine the optical characteristics of sea water, phytoplankton and other components that cause these changes. The roles of inelastic scattering and air bubbles will also be briefly mentioned. Aspects related to the polarization of the scattered light will be omitted (e.g., Morel 1994 and references therein).

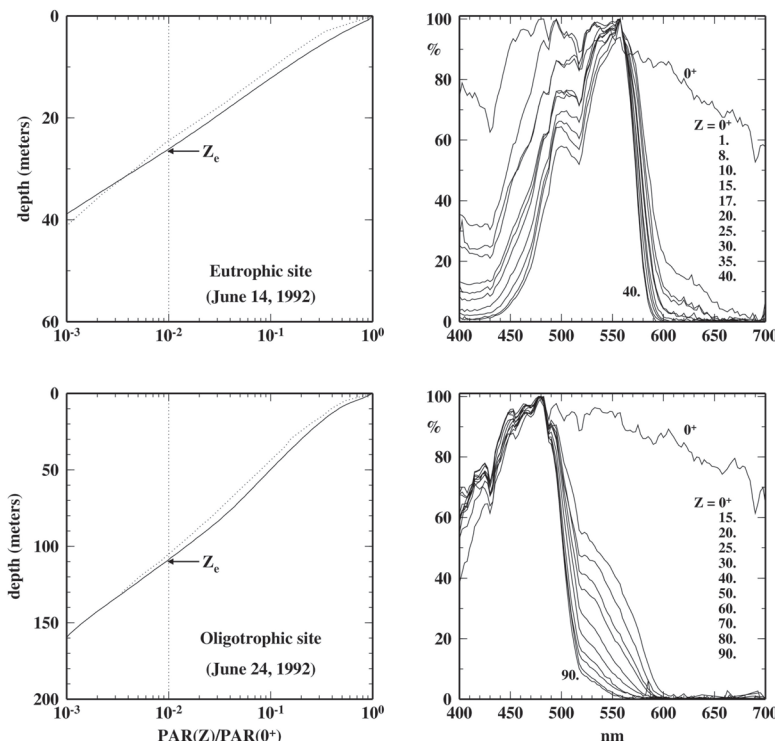


Figure 4-6 Spectra of the downwelling irradiance normalized to their maximum, in “blue” chlorophyll-poor waters (bottom right), and “green” chlorophyll-rich waters (top right), at the depths indicated (0^+ means just above the sea surface). The data have been obtained at two stations off Africa, the latter being the closest to the coast (in an upwelling area), and the former within the north Atlantic oligotrophic gyre. The left panels show the corresponding profiles of the total irradiance between 400 and 700 nm (the so-called Photosynthetically Available Radiation, PAR), with indication of the euphotic depth, Z_e (i.e., the depth where PAR is reduced to 1% of its surface value). The vast majority of the primary production occurs in this layer. After Morel et al. 1996.

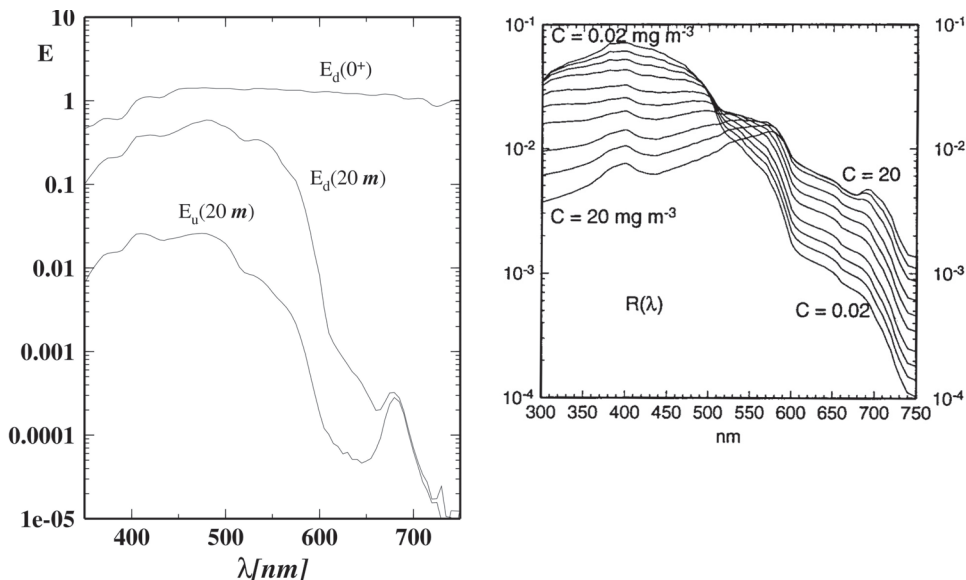


Figure 4-7 Left panel: Spectra of the downwelling irradiance (E_d) and the upwelling irradiance (E_u), as collected at 20 m in moderately clear oceanic waters; they clearly display the peak formed by the fluorescence emission of phytoplankton around 683 nm. Right panel (Source: Morel and Antoine 1994): modelled spectra of the diffuse reflectance, R , for various chlorophyll concentrations (from 0.02 to 20 mg(Chl) m⁻³), as predicted from a semi-analytical bio-optical model (Morel 1988; fluorescence is not included here). These spectra illustrate the change of the underwater radiation, from a domination of the blue wavelengths to a more “green ambience.” They also show the “hinge point” located around 510–520 nm (Clarke et al. 1970) where the variations of R are minimum. Left panel courtesy: David Antoine. Right panel source: Morel, A. and D. Antoine 1994; © American Meteorological Society.

4.3.2.2 ABSORPTION, SCATTERING, AND BACKSCATTERING BY PURE SEA WATER

Sea water causes both absorption (Figure 4-8) and scattering (Figures 4-8 and 4-9). Molecular scattering in sea water is described by the theory of Einstein-Schmoluchowski, according to which the scattering is possible thanks to density fluctuations. According to the theory of Rayleigh, without these fluctuations, scattered radiation from molecules acting like “radian dipoles” would be cancelled by interference. The phenomenon is accentuated in sea water, compared to pure water, by fluctuations in concentration of the various ions. The few measurements of the scattering function (a delicate measurement to carry out), and the more numerous measurements of the scattering coefficient and its spectral dependence, agree with this theory (Morel 1974; Buiteveld et al. 1994). The scattering function of pure sea water can be described by (Morel 1974)

$$\bar{\beta}_w(\theta) = \frac{3}{4\pi(3+p)} (1 + p \cos^2(\theta)) \quad (4-4)$$

where the factor of polarization at 90°, p , is 0.84 (related to the anisotropy of the molecules). The scattering function is symmetrical with respect to the incident direction so that backscatter is half the total, and the backscattering coefficient, b_{bw} , is exactly half the scattering coefficient b_w , with the same spectral dependence. The integration of this function over all solid angles gives the total scattering coefficient, whose spectral dependence is expressed according to a power law, roughly $\lambda^{-4.3}$ (Morel 1974), which increases very quickly as wavelength decreases. This dependency explains why the purest sea waters (Sargasso Sea for instance) have an indigo-blue color.

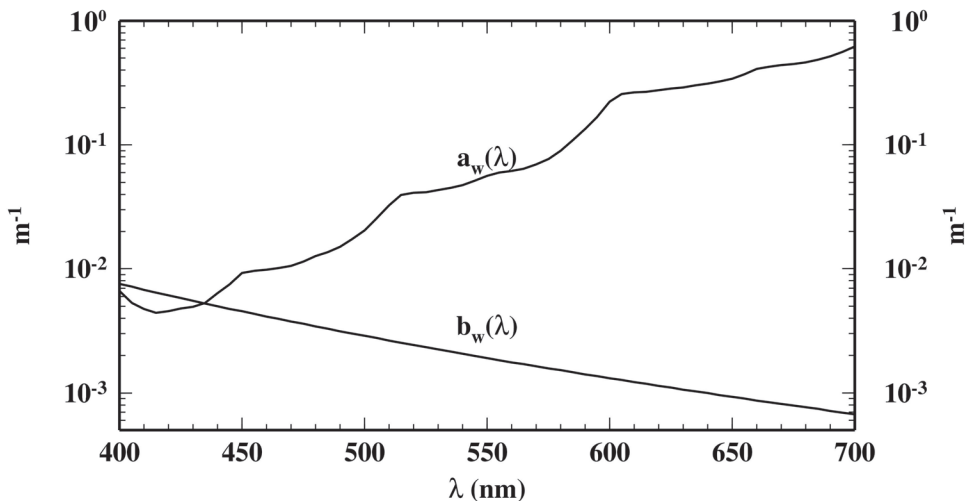


Figure 4-8 Spectra of the absorption (data from Pope and Fry 1997) and scattering (data from Morel 1974) coefficients for pure sea water.

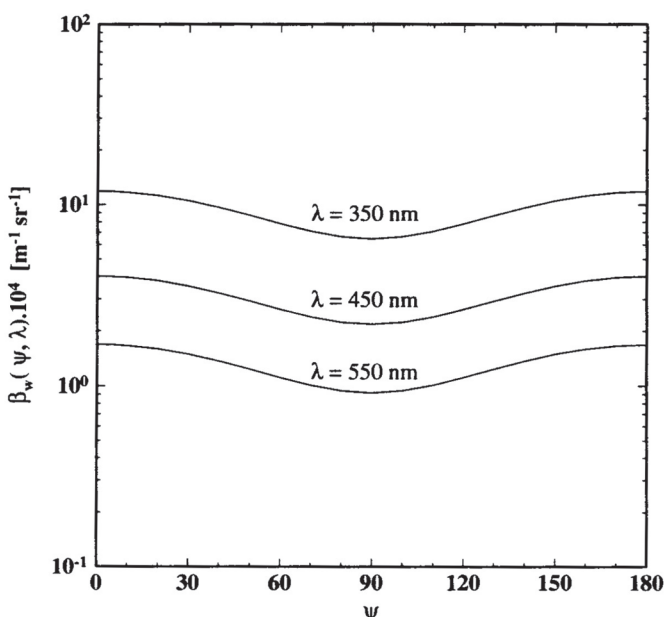


Figure 4-9 Volume-scattering function of sea water at three wavelengths. Source: Figure 1.5 in Loisel 1999. Courtesy: Hubert Loisel.

The absorption spectrum of pure water is also difficult to measure, and values have been revised several times. The latest were obtained by Pope and Fry (1997) and Sogandares and Fry (1997). These replace those of Smith and Baker (1981) and are shown in Figure 4-8. It is worth noting the very weak absorption in the blue compared to the very strong increase at “red” wavelengths. This combines with scattering to give the indigo color of “pure” sea waters. The successive “shoulders” of the spectrum are the signature of the harmonics related to the natural vibrations of the OH bond. Finally, it should be noted that in the red and the infrared domains ($\lambda > 600$ nm), absorption increases slightly with the temperature (Pegau and Zaneveld 1993).

4.3.2.3 ABSORPTION BY PHYTOPLANKTON AND ASSOCIATED PARTICLES AND DISSOLVED SUBSTANCES

The absorption spectrum of phytoplankton (Figure 4-10) results from the superposition of absorption spectra from different pigments, merged in an extremely variable manner according to the species considered and the depth in the water column. The principal pigments are chlorophylls, in particular chlorophyll-a, present in all photosynthetic organisms, and carotenoids. Each has specific absorption bands, as defined by their molecular structure. Chlorophyll-a has two main areas of absorption, in the blue around 440 nm ("Soret" or "B bands") and in the red towards 675 nm ("Q bands"). The carotenoids, which include many pigments, absorb in the blue and blue-green. The combined effect of chlorophylls and carotenoids is the transition in water color from blue towards green when the concentrations of these pigments increase. Rarer pigments, specific to certain species, also contribute and can be significant when the species in question live where illumination is significant in the spectral area in question. This is the case for phycobilins present in cyanobacteria, which absorb in the "green-yellow" domain, around 550 nm (Figure 4-10). The changes of the a_ϕ spectrum are thus mainly due to the variations of the species group. It also varies with the "package effect," in which the effectiveness of absorption changes according to the discreteness of pigments in the organisms, and therefore with intracellular pigment concentration and cell size.

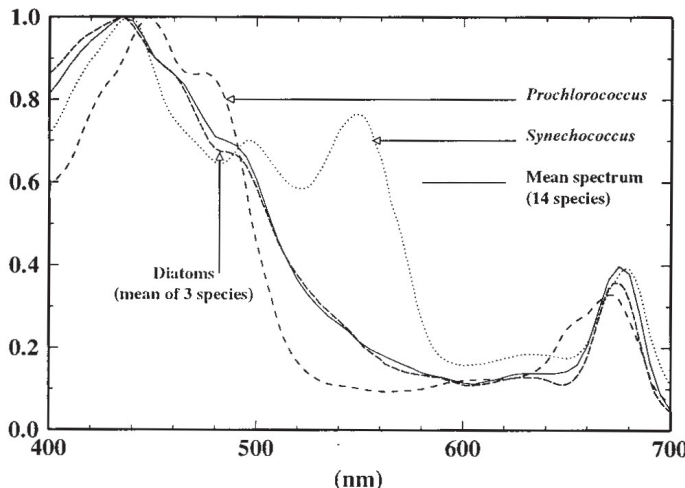


Figure 4-10 Absorption spectra, normalized to their maximum, for various phytoplankton species, as indicated. Synechococcus is a species part of the cyanobacteria group. Source: Antoine and Morel 1996.

One can also study how a_ϕ varies with the chlorophyll concentration, Chl, at a given wavelength, using simultaneous measurements of a_ϕ and Chl (Figure 4-11). It appears then that a_ϕ varies with Chl according to a power law (for example, Bricaud et al. 1995, 1998)

$$a_\phi = A [Chl]^B \quad (4-5)$$

where the coefficient "A" and the exponent "B" vary with the wavelength. The exponent B varies between 0.6 and 1 in the visible spectrum. The non-linearity of Equation 4-5 expresses the changes in pigment composition and package effect, which can result from interspecific variations or from the photo-acclimation in a given population. One can establish the same type of relationship for the specific absorption coefficient ($a_\phi/[Chl]$)

$$a_\phi^* = A [Chl]^{B-1} \quad (4-6)$$

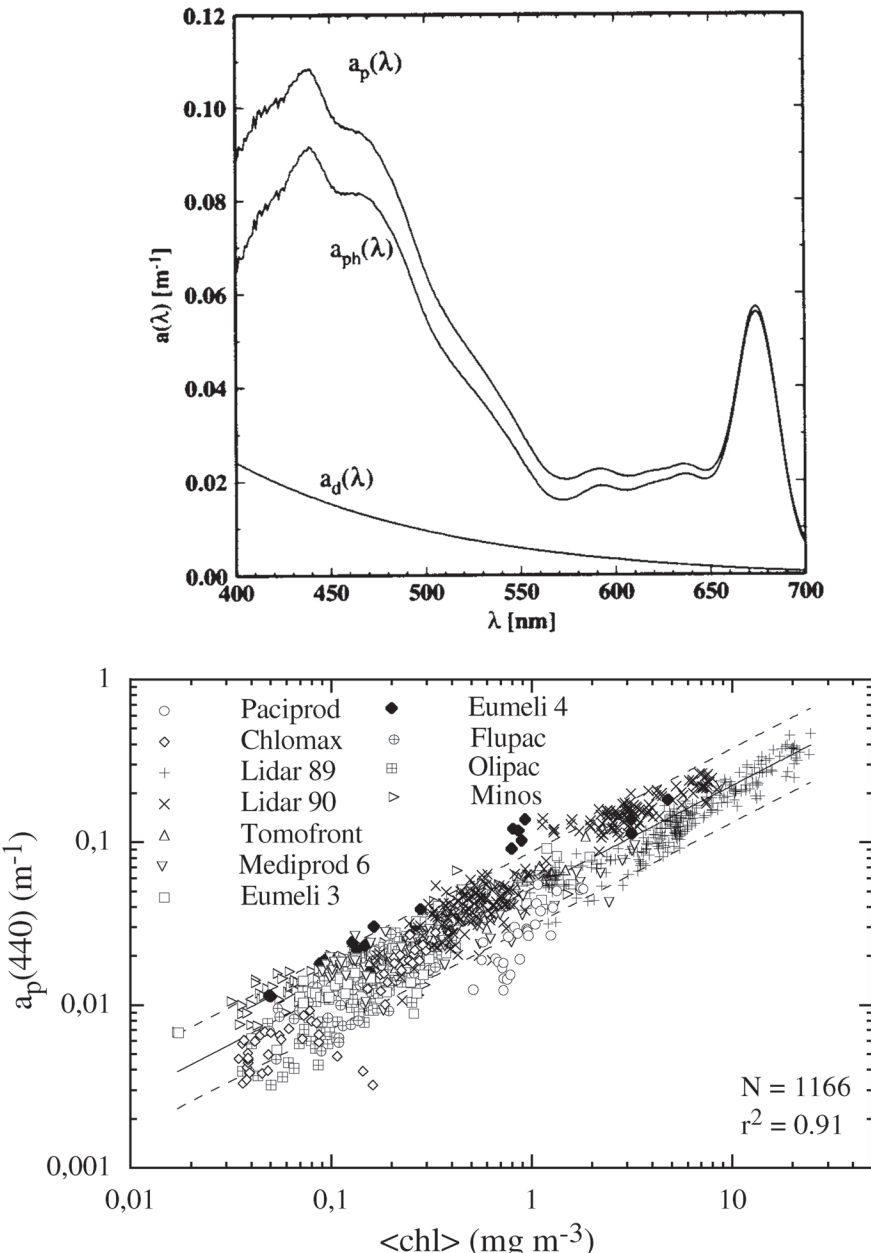


Figure 4-11 Top panel: example of absorption spectra for total particles (a_p), phytoplankton (a_{ph}), and detritus (a_d). Bottom panel: absorption coefficient for total particles at 440 nm, as a function of the chlorophyll concentration. The data are from various cruises in the world ocean, as indicated. Top panel source: Figure 1.3 in Loisel 1999; courtesy: Herbert Loisel. Bottom panel source: Figure 1a in Bricaud et. al 1998.

One would expect that a specific coefficient would be the unique property of a given type of particle. The fact that it is a function of the chlorophyll concentration in Equation 4-6 comes from the consideration here of the full range of variation of the populations of marine particles.

A range of “non-algal” particles is attached to phytoplankton, which includes heterotrophic bacteria and other organisms and the detritus produced by all these organisms.

The former being more or less transparent, they have little importance in absorption. The absorption coefficient of the non-algal particles (Figure 4-11) can, in the same way as a_{ϕ} , be expressed at a certain wavelength by a nonlinear relationship with [Chl], and then its spectrum is described in a satisfactory way by an exponential law of the form

$$a_{nap}(\lambda) = a_{nap}(\lambda_0) \exp(-S(\lambda - \lambda_0)) \quad (4-7)$$

where λ_0 is a wavelength of reference (440 nm in general) and S the slope of the relationship, on average equal to about 0.011 (Bricaud et al. 1998).

Lastly, the colored dissolved substances (commonly called “yellow substances,” “Gelbstoff” or “CDOM” for “Colored Dissolved Organic Matter”) contribute to absorption. Their structure and generally high molecular weight result in an absorption that increases in an exponential way towards short wavelengths as in Equation 4-7, while the slope is now 0.014 on average (Bricaud et al. 1981)

$$a_{ds}(\lambda) = a_{ds}(\lambda_0) \exp(-S'(\lambda - \lambda_0)) \quad (4-8)$$

In addition, the value of a_{ds} at a wavelength of reference (440 nm also) is sometimes expressed as a fraction of the sum ($a_w + a_p$) at the same wavelength, to represent the increase in the concentration of dissolved substances with the concentration of particles, as well as a minimum background of yellow substance even in the clearest waters (Prieur and Sathyendranath 1981).

4.3.2.4 SCATTERING AND BACKSCATTERING BY PHYTOPLANKTON AND ASSOCIATED PARTICLES

The scattering by marine particles, whose sizes range from slightly lower to much higher than the wavelengths of visible and infrared light (0.4 to 1 μm), results from the combined action of diffraction, reflection and refraction (when the index of refraction is different from that of the surrounding medium). The Mie theory makes it possible to describe this scattering by assuming spherical particles, homogeneous in index of refraction, which is, in general, a good approximation for populations of marine particles. Generally the shapes fit in a sphere of diameter comparable with the average size of the particles, and their random orientation makes the assumption more representative. When the index of refraction of the particles is not very different from that of the surrounding medium, the theory can be simplified by “the anomalous diffraction approximation” developed by Van de Hulst (1957). This allows the efficiency factors of scattering and absorption to be calculated, but not the volume-scattering function. A detailed description of these theories and their application to marine particles can be found, for instance, in Morel and Bricaud (1986), Bricaud and Morel (1986), and Morel (1991b).

For typical populations of marine particles, strongly poly-dispersed in terms of size and index of refraction, the resulting volume-scattering function is strongly asymmetrical, with a high scattering at small angles (forward scattering being due to the large particles), relatively stable values perpendicular to the incident direction, and high variability in backscatter. This backscatter is especially due to small particles. The variability is mainly due to changes in index of refraction. Examples of measured volume-scattering functions are shown in Figure 4-12.

The total particle-scattering coefficient, b_p , at 550 nm can be related to chlorophyll concentration by a non-linear relationship (Equation 4-9), with an exponent between 0.6 and 0.8 (Morel 1980; Gordon and Morel 1983; Loisel and Morel 1998). This difference

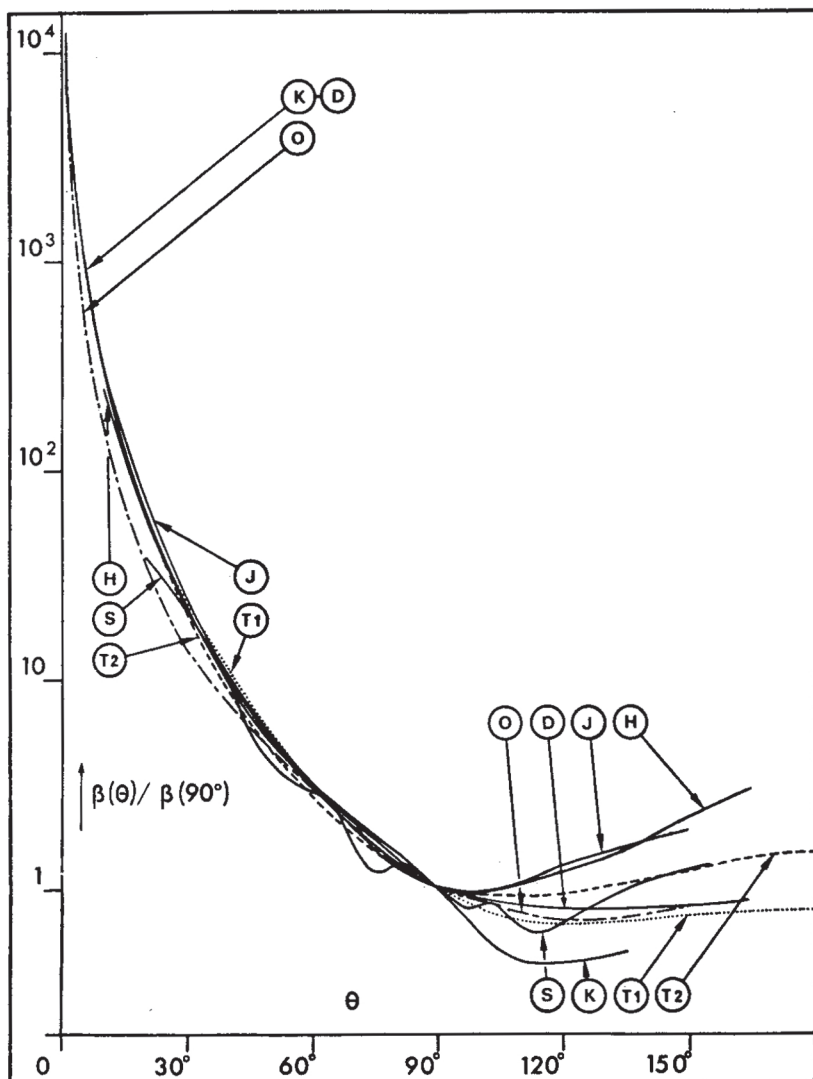


Figure 4-12 Various determinations of the volume-scattering function of sea waters, and normalized at 90° . H: E. O. Hulbert (1945), Chesapeake Bay. K: M. Kozlianinov (1957), China Sea. S: T. Sasaki et al. (1960), deep ocean near Japan. J: N. G. Jerlov (1961), Atlantic (Madeira). T₁/T₂: J. E. Tyler (1961), Pacific (San Diego). D: S. Q. Duntley (1963), Winnipesaukee Lake. O: Y. E. Otschakovski (1965), Mediterranean Sea. Source: Figure 12 in Morel 1973.

from 1 expresses both the variability of the specific scattering coefficient of phytoplankton, and the increasing importance of non-algal particles when the chlorophyll concentration decreases (Figure 4-13)

$$b_p(550) = 0.30(\pm 0.15) [Chl]^{0.7(\pm 0.1)} \quad (4-9)$$

The spectral dependence of b_p can be described by a power law whose exponent ($\text{\AAngstr\"om exponent}$) varies mainly with the size distribution of the particles (from approximately 0 when the large particles dominate, to higher values when the contributions of

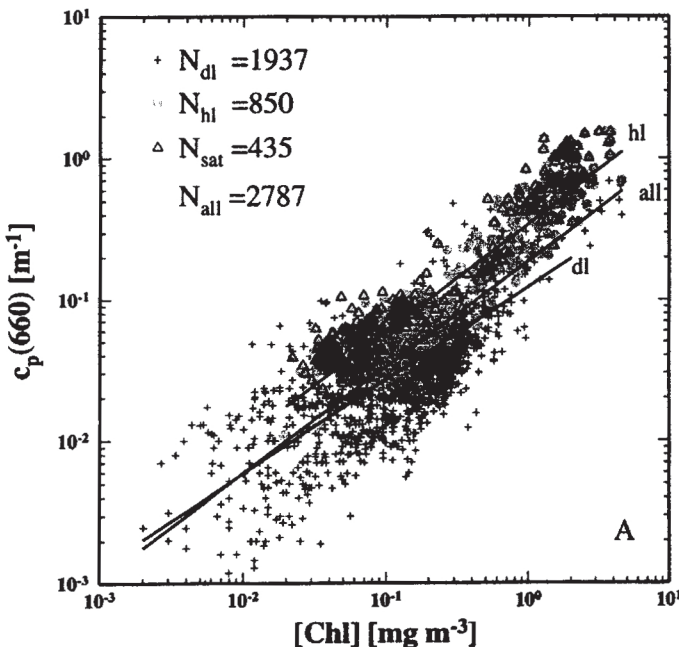


Figure 4-13 Attenuation coefficient of particles at 660 nm as a function of the chlorophyll concentration. Attenuation is mostly due to scattering since absorption is weak at this wavelength. Source: Figure 3A in Loisel and Morel 1998. Copyright 1998 by the American Society of Limnology and Oceanography, Inc.

small particles increase). An average value usually used is $n = -1$. If the distribution follows a Jüngé law with an exponent v , then $n = 3 - v$.

$$b_p(\lambda) = b_p(550) (\lambda / 550)^n \quad (4-10)$$

For reflectance, backscatter is the important factor. For marine particles, the ratio between backscatter and total scatter, $\tilde{b}_b = b_b/b$, is highly variable and still badly known. Several parameterizations have been proposed (Morel 1988; Gordon et al. 1988b). Better understanding of this variability is one of the major challenges of marine optics.

4.3.2.5 INELASTIC SCATTERING (RAMAN AND FLUORESCENCE)

In inelastic scattering, the re-emission of radiation occurs with loss of energy and thus at a longer wavelength than that of excitation. In the case of Raman scattering, re-emission takes place at symmetrical frequencies about a central exciting frequency, the positions of which are determined by the characteristics of atomic bonds. One must define both the excitation spectrum and the emission spectrum for Raman scattering. Emission at longer wavelengths has a symmetrical scattering function (like that of the Rayleigh scattering) and a spectral dependence approximately as λ^{-5} . The relative effect of this phenomenon on $R(\lambda)$ is more significant at longer wavelengths ($\lambda > 550$ nm) and at low chlorophyll concentrations. It can reach 10% of $R(\lambda)$ (see Mobley 1994).

Phytoplankton fluorescence is due to the chlorophyll-a molecule. The radiative energy collected by photosynthetic pigments in the visible spectrum can follow two paths, or can be lost as heat. It is either transmitted to the chlorophyll molecule and then transferred sequentially within the photosynthetic apparatus (primary production), or it is re-emitted as fluorescence in a small range of wavelengths, centered on 683 nm. This second path will be

used when the photosynthetic apparatus is saturated and cannot accept more energy. Fluorescence is thus a function of both the chlorophyll-a concentration and of the physiological state of the phytoplankton (specifically of the photosynthetic apparatus).

A peak centered at 683 nm is often a clear feature of spectra of upwelling irradiance measured at sea (Morel and Prieur 1977; Gordon 1979; see Figure 4-7). This natural fluorescence may help to quantify chlorophyll from space measurements (Babin et al. 1996; Gower et al. 1999), as an alternative to the more traditional methods based on differential absorption in the blue and green domains. This could be especially useful in Case 2 waters where these techniques fail. However, the physiological state of the phytoplankton would have to be known for an accurate result.

4.3.2.6 THE SCATTERING BY AIR BUBBLES

The role of air bubbles in the surface layers was regularly evoked to explain part of the backscattering of sea waters (Stramski 1994, for instance), but it is only recently (Zhang et al. 1998) that their effect was shown to be significant. These bubbles, created by breaking waves, can persist a long time after the causes of their generation have disappeared. Their size varies from approximately 0.1 to 10 μm , and they contribute to backscattering, especially in chlorophyll-poor waters. The presence of an organic film at their surface also increases their backscatter. Uncertainties persist about their contribution, in particular because their size distribution and total number per unit volume are difficult to assess.

4.3.2.7 IN SHORT

The biophysical causes of relationships between optical properties and the chlorophyll concentration also generate a natural noise around these relationships, reflecting the fact that chlorophyll is not in fact the sole determinant of optical properties. One solution can be to establish relationships for restricted geographical or parametric domains (“regionalization”). Another is to try to better understand the causes of variability, and express it using parameters measurable from space, such as temperature, light intensity, or nutrient concentration. Much work is currently underway to advance our understanding of the relationships in these two complementary ways.

4.3.3 Principles of Satellite Ocean Color Remote Sensing

Ocean color remote sensing seeks to quantify the chlorophyll concentration by measurement of radiances above the atmosphere. The three stages of this process, each having its own specific difficulties, are the following: 1) the measurement of radiance above the atmosphere; 2) computation of the radiance leaving the water (correction for the effects of the atmosphere); and 3) the calculation of the chlorophyll concentration and other quantities from this corrected signal.

4.3.3.1 THE MEASUREMENT OF RADIANCE ABOVE THE ATMOSPHERE

An instrument for ocean color remote sensing must record the quantity of radiative energy by converting it into an electrical signal, which is then digitized, processed and/or stored and sent to ground receiving stations. The signal depends on the wavelength and on the angular instantaneous field of view (IFOV) that corresponds to the area of a basic observable element (“pixel”) on the ocean surface. One difficulty faced in the design of these instruments is producing sufficiently high signal-to-noise ratios in spite of the weakness of the signal observed. The measured signal corresponds to the total radiance from a given

direction, determined by the optical properties of the ocean, the air-to-sea interface, and, most importantly, the atmosphere, including clouds if they are present.

4.3.3.2 THE VARIOUS CONTRIBUTIONS TO THE TOTAL RECORDED SIGNAL

The Total Radiance L_T

The total radiance received by the sensor above the atmosphere, L_T , can be broken down as follows (omitting spectral and angular dependencies):

$$L_T = L_R + L_A + L_{RA} + L_G + L_F + tL_W \quad (4-11)$$

Each term is presented in the following paragraphs (see also the Table of Symbols), and is illustrated in a diagrammatic way in Figure 4-14. Figure 4-15 shows the geometry of the problem.

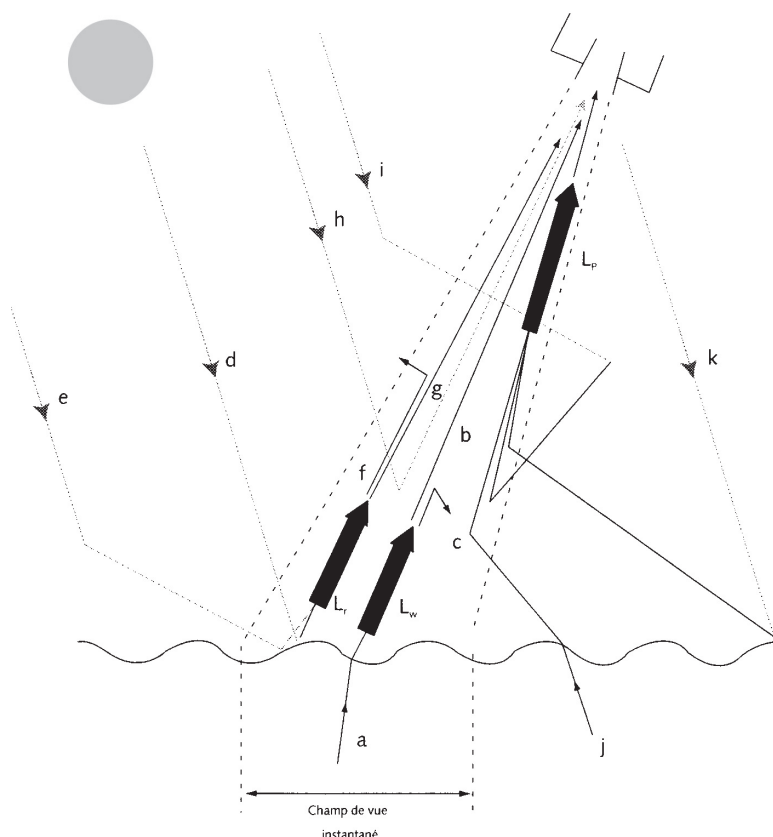


Figure 4-14 Various contributions to the total radiance recorded by a satellite-borne sensor. (a, b, c): water-leaving radiance and its transmission through the atmosphere; (d, e, f, g and k): various combinations of scattering in the atmosphere plus reflection at the sea surface; (h): single scattering in the atmosphere; (i): multiple scattering in the atmosphere; (j): environment effect (i.e., radiance coming from outside of the instantaneous field of view). Reproduced from Antoine 1998; Modified from Robinson 1983.

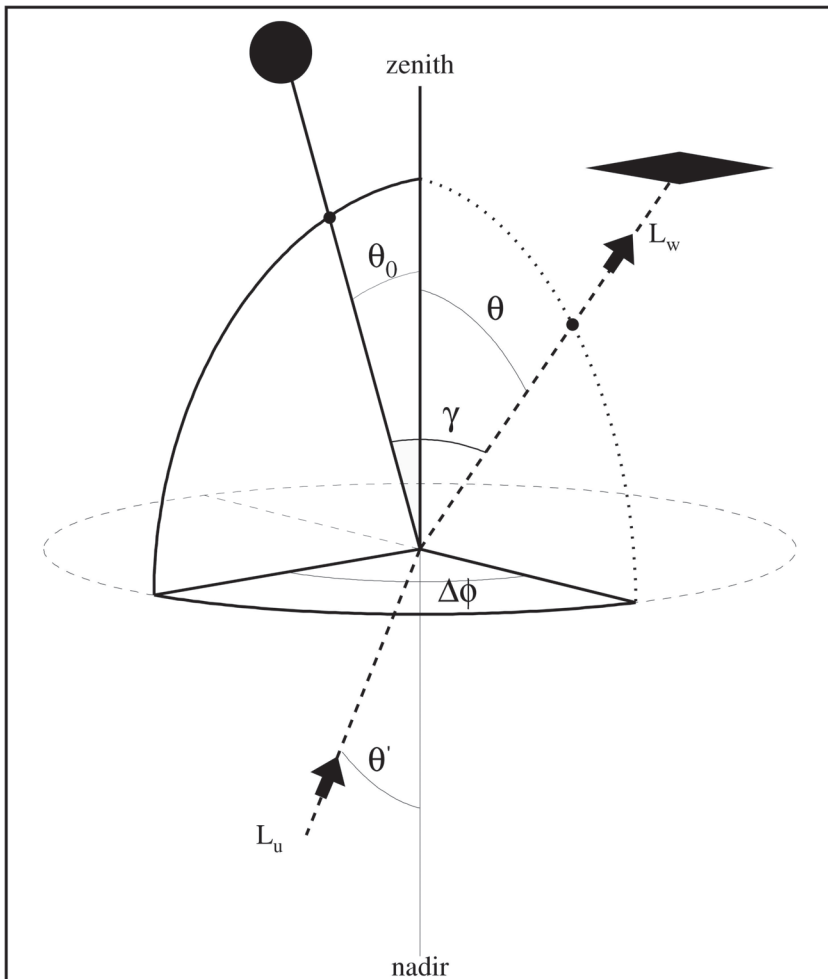


Figure 4-15 Geometry of the remote-sensing problem (cf., Table of Symbols). Source: Figure 1 in Morel and Gentili 1996. Courtesy: OSA.

The Water-leaving Radiance, L_w

The contribution at the sensor level of the photons having penetrated in the ocean is expressed by the product of the radiance exiting the ocean, L_w (the “water-leaving radiance”), and the diffuse transmittance of the atmosphere, $t(\lambda, \theta)$. An approximate empirically established formulation is given below:

$$tL_w = t(\lambda, \theta) L_w(\lambda, \theta_0, \theta_v, \Delta\phi) \quad (4-12)$$

where t can be approximated by

$$t(\lambda, \theta) = \exp \left[- \left(\frac{1}{2} \tau_R(\lambda) + \frac{1}{6} \tau_A(\lambda) + \tau_{ag} \right) / \cos(\theta) \right] \quad (4-13)$$

The τ 's are the optical thicknesses of the atmosphere (molecules, τ_R , and aerosols, τ_A), and the absorbing gases (τ_{ag}), mainly ozone. The factor 1/2 is exact and accounts for the symmetry of the volume-scattering function of the air molecules, while the factor 1/6 (undoubtedly a maximum) (Viollier 1980) is an approximation and indicates its strong asymmetry for aerosols. This makes their impact on the transmittance negligible as long as their optical thickness is low (Gordon 1984). The oceanic contribution to L_T is typically lower than 10%. For increasing chlorophyll concentrations, L_w can become almost zero at 445 nm. The causes of L_w variations have already been examined.

The penetration depth (Z_{90}) is an important parameter for understanding marine radiances. It can be defined, in the case of a vertically homogeneous ocean, as the depth where illumination is reduced to 1/e of its value at the surface

$$\int_0^{Z_{90}(\lambda)} K_d(\lambda, z) dz = 1 \quad (4-14)$$

where K_d is the diffuse attenuation coefficient, and $Z_{90}(\lambda)$ is the depth of the oceanic layer that contributes to 90% of the water-leaving radiance, L_w . Gordon and McCluney (1975) showed that a good approximation of $Z_{90}(\lambda)$ was given by the inverse of the diffuse attenuation coefficient. The practical consequence of these definitions is that a sensor located above the surface will not be able to "see" below the penetration depth. Attenuation increases with pigment concentration, making the layer contributing to L_w thinner. This layer depth also varies with wavelength. The influence of the vertical stratification of optical properties on this penetration depth is negligible (André 1992).

Molecular (Rayleigh) Scattering by Air Molecules, L_R

This term includes photons reaching the sensor from the sun after being scattered a certain number of times by molecules in air and possibly also reflected by the sea surface. A possible L_R expression is given below, following the single-scattering assumption (spectral and angular dependencies are omitted or simplified; see Table of Symbols at the end of the chapter for explanations of terms)

$$L_R(\lambda, \theta_0, \theta_v, \Delta\phi) = \left[\frac{F_0 \mu_0 \omega_R}{\mu_v + \mu_s} p_R(\gamma^-) (1 - e^{-\tau_R(1/\mu_v + 1/\mu_0)}) \right] + \\ \left[\frac{F_0 \mu_0 \omega_R}{\mu_s - \mu_v} p_R(\gamma^+) \rho_F(\theta_v) e^{-\tau_R/\mu_v} (e^{-\tau_R/\mu_0} - e^{-\tau_R/\mu'}) \right] + \\ \left[\frac{F_0 \mu_0 \omega_R}{\mu_s - \mu_v} p_R(\gamma^+) \rho_F(\theta_s) e^{-\tau_R/\mu_0} (e^{-\tau_R/\mu'} - e^{-\tau_R/\mu_v}) \right] \quad (4-15)$$

The three terms of this equation, respectively, account for (see Figure 4-16)

- A. photons having undergone one scattering in the atmosphere without interaction with the sea surface ($\theta_O = \theta_v$),
- B. photons scattered once, reflected by the sea surface, then returned directly towards the sensor (θ is the angle between the zenith and the direction of incident photons),
- C. photons reflected at the sea surface, then scattered towards the sensor (θ' is the angle between the zenith and the direction in which the photon is considered).

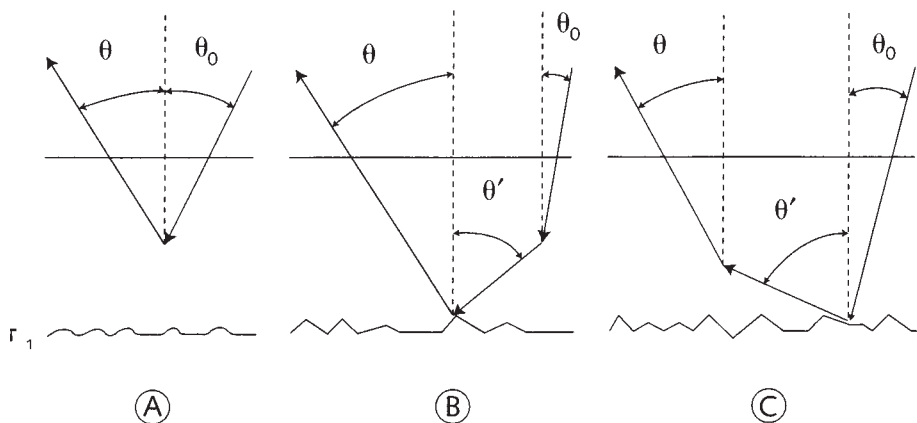


Figure 4-16 The various contributions to the single-scattering radiance (molecular or aerosol scattering). Source: Figure A1 in Wang 1991. Courtesy: Menghua Wang.

If the optical thickness is sufficiently small and the ocean-atmosphere interface is perfectly flat (the angles θ and θ_v are then equal in the 2nd term, and the angles θ and θ_0 are equal in the 3rd term), this expression is simplified (using $1 - e^{-x} \sim x$ for small x) to

$$L_R(\lambda, \theta_0, \theta_v, \Delta\phi) = F'_0(\lambda) \tau_R(\lambda) \varpi_R(\lambda) p_R(\lambda, \gamma\pm) / 4\pi \cos(\theta_v) \quad (4-16)$$

where

$$F'_0(\lambda) = F_0(\lambda) \exp \left[-\tau_{O3}(\lambda) \left(\frac{1}{\cos(\theta_0)} + \frac{1}{\cos(\theta_v)} \right) \right]$$

and

$$p_R(\lambda, \gamma\pm) = P_R(\gamma\pm, \lambda) + [\rho_F(\theta_v) + \rho_F(\theta_0)] P_R(\gamma\pm, \lambda)$$

The $P_R(\gamma\pm, \lambda)$, is the symmetrical Rayleigh phase function. ρ_f is the Fresnel coefficient for the direction θ . $\gamma\pm$ is the scattering angle (see Table of Symbols).

If the single-scattering assumption is abandoned (scattering can be then of all orders), the L_R calculation involves solving the radiative transfer equation (for example, Gordon et al. 1988a; Gordon and Wang 1992a, b), and there is no longer any simple analytical expression. The spectral change of L_r is following a $\lambda^{-4.09}$ law.

At given wavelength and geometry of observation, L_R varies with atmospheric pressure that determines the quantity of molecules in the atmosphere. In the single-scattering regime, L_R is directly proportional to the pressure, via the optical thickness τ_R . In the case of the multiple scattering, the relationship is not linear (Gordon et al. 1988a). The influence on L_R of a sea surface roughened as a function of wind speed (Plass et al. 1975) was estimated for the CZCS (Gordon and Wang 1992a, b). It is of the same order of magnitude as the result of a variation of ± 15 mb in pressure, or ± 50 "Dobson Units" of ozone (Andre and Morel 1989).

Aerosol Scattering, L_A

This term represents photons scattered a certain number of times by aerosols. As with L_R , there is an expression valid under the single-scattering assumption (only one collision with

an aerosol). The expression is identical to that of the Rayleigh scattering, with a phase function $P_A(\gamma \pm, \lambda)$, which can be derived from the Mie theory if the characteristics of the aerosols are known (index of refraction and size distribution, both being modified by moisture).

$$L_A(\lambda, \theta_o, \theta_v, \Delta\phi) = F'_0(\lambda) \tau_A(\lambda) \varpi_A(\lambda) p_A(\lambda, \theta_o, \theta_v, \Delta\phi) / 4 \pi \cos(\theta_v) \quad (4-17)$$

If the single-scattering assumption is abandoned, the calculation again requires solving the radiative transfer equation, and again there is no longer any simple analytical expression. The spectral change of L_A is following a λ^{-n} law, with n from about 0 to 2.5.

L_A is more variable than L_R , and the significant factors are more numerous. The aerosol optical thickness is the major source of variation, and in addition, the phase function depends on the index of refraction, the size distribution, and the humidity of the aerosols. The great spatial and temporal variability of these atmospheric particles makes L_A , in general, not directly calculable for a satellite observation. Only indirect methods are possible (see 4.3.3.3).

Coupled Molecular-aerosol Scattering, L_{RA}

It is conceivable that photons penetrating in the atmosphere can be successively scattered by molecules and aerosols, and that the two terms previously described ($L_R + L_A$) are not enough to characterize the complete radiative regime (Deschamps et al. 1983). A coupling term, L_{RA} , is then added, which can be of the same order of magnitude as L_A . There are two different ways of tackling this problem.

One can consider the L_R value such as it would be for an atmosphere without aerosols (purely molecular), and the value of L_A for a hypothetical atmosphere without molecules (only aerosols). In both cases one can consider multiple scattering. When one adds these two contributions to compute L_T , the additional L_{RA} term, most of the time negative, expresses the fact that the two radiances L_R and L_A actually overestimate the value in a realistic atmosphere. This is the approach used by Deschamps et al. (1983) and Gordon and Wang (1994).

Alternatively, one can calculate the three terms L_R , L_A and L_{RA} for realistic atmospheres (molecules + aerosols) using a “Monte Carlo” simulation of the radiative transfer, following the paths of all photons injected into the ocean-atmosphere system, defined beforehand by its optical properties and suitable boundary conditions (Antoine and Morel 1998). In this case, one can calculate the exact value of the coupling term L_{RA} and analyze scattering events that dominate in its generation.

Specular Reflection at the Sea Surface, L_G

This “glitter” term concerns photons that undergo no scattering in the atmosphere, only reflection at the sea surface. Some ocean color sensors have the possibility of tilting their observations to avoid the direction that corresponds to this specular reflection of the sun. This direction is well-defined if the sea surface is perfectly flat (actually the apparent angular size of the sun disk, i.e., about 0.5°). The reflection can then cause saturation of the instrument. If the surface is not perfectly flat, other viewed directions can be “contaminated” by the specular reflection signal. In this case it is useful to calculate this signal to provide valid data over a larger area of ocean. L_G is a function of the geometry of the observation and of the sea surface state. A possible expression is (Vermote et al. 1997)

$$L_G(\lambda, \theta_o, \theta_v, \Delta\phi) = F_0(\lambda) \cos(\theta_o) P(\theta_o, \theta_v, \Delta\phi) \rho_F(n, \theta_o, \theta_v, \Delta\phi) / 4 \pi \cos(\theta_v) \cos^4(\theta_n) \quad (4-18)$$

where P is a function describing the Gaussian, isotropic, distribution of the waves facets (Cox and Munk 1954), ρ_F is the Fresnel reflection coefficient, and θ_n the zenith angle of the facet with respect to the sun.

Contribution due to Whitecaps, L_F

This term can be significant (up to 5%) at high wind speeds (Gordon and Jacobs 1977). According to Koepke (1984), the reflectance of sea foam would be spectrally neutral and proportional to the fraction of the surface covered by foam, W , ($W \cdot \rho_{ef}$, with $\rho_{ef} \sim 22\%$). W can be expressed as a function of wind speed, U (Monahan and O'Muircheartaigh 1980)

$$W = 2.95 \cdot 10^{-6} U^{3.5} \quad (4-19)$$

a possible expression of L_F is then (Vermote et al. 1997)

$$L_F(\lambda, \theta_0, \theta_v, \Delta\phi) = F_0(\lambda) \cos(\theta_0) W \rho_{ef} / \pi \quad (4-20)$$

Frouin et al. (1996) showed that the reflectance spectrum of sea foam is not neutral, with a notable reduction for wavelengths longer than about 800 nm. This could affect calculation of the spectral dependence of aerosol scattering, which is based on the signals at these wavelengths (see Section 4.3.3.3).

4.3.3.3 THE ATMOSPHERIC CORRECTION

In order to analyze the light backscattered by the ocean, it is necessary to extract from total radiances (L_T) the part that comes from the ocean, referred to as the “marine radiances” (L_W). The necessary operations, “atmospheric corrections,” consist of eliminating the part of the radiation that was backscattered by the molecules (L_R) and aerosols in the atmosphere (L_A and L_{RA}), possibly also reflected at the ocean surface (L_G and L_F), but never penetrated the ocean. Many papers have been written on this subject, and we only outline the existing techniques here. They are in general based on a decomposition of the signal (Equation 4-11).

Here, we omit the effect of absorption, since most instruments observe out of the principal atmospheric absorption bands. Where it is significant, the measured signals can be corrected to their value in the absence of such absorption. The simplest technique would neglect the coupling between absorption and scattering. When it is significant, multiple scattering increases apparent absorption by increasing the photon’s path lengths.

The signal due to scattering by molecules can be accurately estimated if the atmospheric pressure (defining the quantity of molecules in the atmospheric “column”), and the volume-scattering function of the molecules are known. The effects of polarization and modification of the way in which illumination is reflected at the air-to-sea interface can be taken into account (Gordon et al. 1988a; Gordon and Wang 1992a, b).

Aerosol scattering causes greater difficulties, since neither concentration nor volume-scattering function are known *a priori*, i.e., before carrying out the correction of the signal. Horizontal and vertical distributions of aerosols, and their type, are highly variable parameters. To obtain these two unknown factors, at least two equations are required, which means in practice that information must be obtained at a minimum of two wavelengths.

Most currently used techniques rely on the observation in at least two channels in the near infrared, for which the oceanic signal is zero (at least in Case 1 waters). This is due to the very strong absorption of water itself, and to the low scattering of the various materials present (except perhaps air bubbles, a recently raised difficulty). After correction for mo-

lecular scattering, the remaining signal at these wavelengths is entirely due to aerosols. From the intensity of this signal and its spectral dependence between the two wavelengths, the aerosol contribution can be extrapolated through visible wavelengths (for example, Gordon 1978; Bricaud and Morel 1987; Andre and Morel 1991; Gordon and Wang 1994; Fraser et al. 1997; Gordon 1997; Antoine and Morel 1998, 1999).

4.3.3.4 THE INVERSION OF THE MARINE RADIANCES SPECTRUM

The marine radiances obtained after atmospheric correction can be expressed by the following equation (see Table of Symbols):

$$L_w(\lambda, \theta_s, \theta', \Delta\phi) = E_d(0^+) \mathfrak{R}(\theta') \frac{f(\lambda, \theta_s)}{Q(\lambda, \theta_s, \theta', \Delta\phi)} \left[\frac{b_b(\lambda)}{a(\lambda)} \right] \quad (4-21)$$

which is obtained by combination of the following definitions (omitting the spectral and angular dependence, and replacing “ $F_{\lambda, \beta}$ ” of Equation 4-1 by the symbol “f”, more often used):

$$R = \frac{E_u}{E_d} = f \frac{b_b}{a} \quad ; \quad Q = \frac{E_u}{L_u} \quad ; \quad L_w = L_u \frac{1 - \rho_F}{n^2} \quad ; \quad E_d(0^-) = E_d(0^+) \frac{1 - \bar{\rho}}{1 - \bar{r} R}$$

Equation 4-21 implies anisotropy in the marine radiance field, in the sense that L_w , and *a fortiori* L_w , do not have the same values at different viewing angles. This anisotropy depends on the shape of the volume-scattering function of marine particles, and also on the ratios $\bar{\omega}$ ($= b/c$) and η ($= b_w/b$). The anisotropy is described by the Q factor, the values of which were first deduced theoretically (Morel and Gentili 1991, 1993, 1996), and then checked in experiments (Morel et al. 1995).

Several solutions exist to deduce the chlorophyll concentration starting from $L_w(\lambda)$. The influence of chlorophyll in Equation 4-21 appears through coefficients b_b and a , and also through the ratio of the f and Q factors. Empirical relationships between values of L_w at various wavelengths, combined in ratios (or ratios of differences) and chlorophyll concentration, can be derived from simultaneous *in situ* measurements of radiances and chlorophyll (e.g., Clark 1981; O'Reilly et al. 1998). The most frequently used empirical algorithms use the “blue/green” ratio, namely the ratio of radiances at wavelengths ~ 440 and ~ 550 nm, two wavelengths that represent the minimum and the maximum of the phytoplankton pigments' absorption (cf., Figure 4-10). The algorithm would become “semi-empirical” if the relationships used were no longer based on measurements but on the results of a model of the optical properties (see Figure 4-17).

Rather than using observed radiances, which are influenced by the geometry of the observation, one can use reflectances R, equal to (Equations 4-1 and 4-21)

$$R(\lambda) = \frac{L_w(\lambda, \theta_s, \theta', \Delta\phi) Q(\lambda, \theta_s, \theta', \Delta\phi)}{E_d(0^+) \mathfrak{R}(\theta')} \quad (4-22)$$

or even normalized radiances, $[L_w]_N$ (Gordon and Clark 1981), i.e., radiances such as these would be observed without atmosphere, and when the sun is at zenith and at its mean dis-

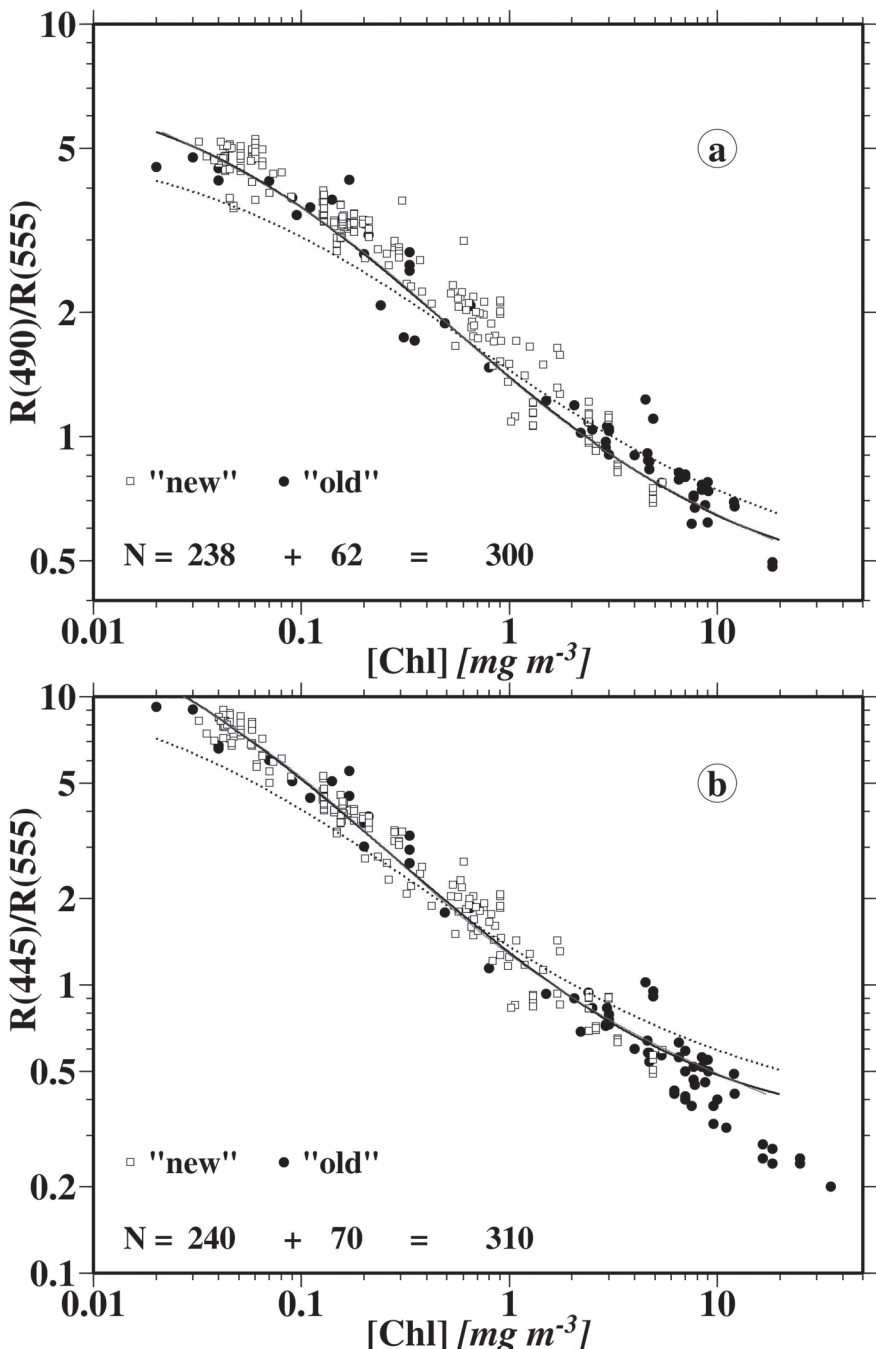


Figure 4-17 Illustrations of the change of two different reflectance ratios (i.e., $R(443)/R(555)$ and $R(490)/R(555)$) with the chlorophyll concentration. The various symbols correspond to data collected in various parts of the world ocean, and the two lines correspond to the bio-optical model proposed in Morel and Maritorena 2001. Source: Figure 11 in Morel and Maritorena 2001.

tance from the Earth (subscript 0 indicates a sun at zenith)

$$[L_w]_N(\lambda) = F_0(\lambda) \mathfrak{R}(\theta') \frac{f_0(\lambda)}{Q(\lambda, \theta_s = 0, \theta', \Lambda\phi)} \left[\frac{b_b(\lambda)}{a(\lambda)} \right] \quad (4-23)$$

The only difficulty when using normalized radiances lies in the calculation of f and Q (or their ratio) since they depend not only on the geometry of the observation (Morel and Gentili 1991, 1993), but also on the chlorophyll concentration itself. This problem can be solved using iterative procedures (Morel and Gentili 1996). Normalized radiometric quantities can then be compared between different satellites, since the angular effects are eliminated.

Lastly, one can choose to use all the available measured spectral values in spectral matching or inverse modeling (for example, Doerffer and Fischer 1994), or in neural networks (procedures of multiple non-linear regressions; Schiller and Doerffer 1999; Keiner and Brown 1999; Gross et al. 2000). These techniques aim to determine which parameter or combination of parameters best reproduces the observed spectrum, with the help of a model connecting the optical properties and the parameter in question. Such techniques are also well-suited to cope with noise of various origins (i.e., radiometric noise, error in atmospheric corrections, biological noise).

4.3.4 Difficulties of Ocean Color Remote Sensing

A major problem in ocean color remote sensing from space is the weakness of the marine radiance signal that one tries to identify, compared to the signal that needs to be eliminated. The marine radiance represents only a maximum of 10% of the total signal measured at the sensor level. The signal to be eliminated is due to the atmosphere and the ocean-atmosphere interface. Aerosols represent the central difficulty in this atmospheric correction. Progress has recently been made, though little is still known of aerosols and their climatology. However, even an excellent atmospheric correction cannot produce good results if the measured signal is not perfectly calibrated. Calibration will not be described in detail here, but its role is crucial for the final quality of the data. This was a major problem for the use of Coastal Zone Color Scanner (CZCS) data, for instance (Evans and Gordon 1994).

Also, the marine radiance signal must be extracted with a very high degree of accuracy if chlorophyll concentration is to be adequately determined. The goal is to detect 30 chlorophyll classes between 0.03 and 30 mg m⁻³, which covers almost the whole range of concentration encountered in the world ocean. The interval is divided into logarithmically equal classes (the distribution of the chlorophyll concentrations in the ocean is quasi log-normal; Campbell 1995). To achieve this goal, one cannot tolerate errors of atmospheric correction higher in absolute value than approximately 0.002 (in terms of reflectance) at 440 nm, namely, an error corresponding at a maximum to 5% of the marine reflectance at this wavelength (Gordon 1997; Antoine and Morel 1999).

There exists significant noise around the simple relationships between optical properties and chlorophyll concentration. This noise originates in the variability of the assemblages of pigments, particles, and dissolved substances that accompany the phytoplankton. The optical properties, and thus L_w , vary in consequence approximately by a factor 2–3 for a given chlorophyll concentration. Many efforts are being made to better describe, understand, and quantify this natural variability that, at the present time, constrains the capabilities of ocean color remote sensing. The problem of Case 2 waters, not treated here, is even more complex insofar as the presence of sediments and exogenic dissolved substances in variable proportions can lead to extremely similar reflectance spectra.

4.4 HOW PRIMARY PRODUCTION IS MODELED FROM SPACE OBSERVATIONS

The first three subsections below relate to the modeling of total primary production from ocean color remote sensing observations. The fourth subsection (4.4.4) provides some information on modeling new production.

4.4.1 From Surface Values to Water-column Integrated Quantities

The issues of inferring depth-resolved information from a measurement that essentially concerns the top surface layers of the ocean (no more than 25 m in extremely clear waters) (Gordon and McCluney 1975) are now examined, before entering into the problem of transforming the information provided by remote sensing, i.e., the phytoplankton stock, into a flux, i.e., the primary production. This is an important problem for ocean color, often encountered in other remote-sensing approaches.

Net photosynthesis occurs as long as a sufficient amount of photons can be trapped by the chlorophyll molecules in antennae of the photosynthetic apparatus and can, therefore, continue at quite deep levels in the ocean. However, the balance between carbon fixation by cells and their respiration (which consumes organic molecules and produces CO₂) defines a limit below which algal growth, hence primary production, is impossible. The depth at which the balance is reached is the “compensation depth” (Sverdrup 1953), rarely greater than about 150 m. Therefore, the problem consists of estimating the vertical profile of chlorophyll concentration in the upper 150–200 m from its value in the top few meters. Fortunately, there exist causal relationships between biomass at depth and biomass at the surface. These have been documented for a long time, actually since measurements of chlorophyll through the fluorometric technique have been developed and become routine.

It is worth recalling the basic phenomena that drive the vertical organization of phytoplankton. In eutrophic, chlorophyll-rich environments (such as upwellings or some coastal areas), abundant nutrients are brought to the surface by vertical mixing, and therefore fertilize the upper layers and sustain healthy and abundant phytoplankton populations. The biomass in that case is mostly uniformly distributed with depth, and if a maximum occurs it is near the surface. At the opposite side of the trophic scale are the chlorophyll-poor environments, referred to as oligotrophic areas. Nearly half of the global ocean surface is located within the two tropical belts in “oligotrophic gyres.” These have extremely low (< 0.05 mg m⁻³) concentrations at the surface and a deep chlorophyll maximum (DCM) determined by the depth of the nutricline. This is the depth where the nutrient concentrations start to increase above levels undetectable to conventional measurement techniques. This depth is mostly determined by a physical barrier to vertical motions, namely, the pycnocline, which restricts upward movement of nutrients, leading to very low concentrations of phytoplankton above it. Between the two end-members, i.e., the DCM of oligotrophic areas and the surface maximum of eutrophic zones, a variety of situations may exist, fortunately following a rather regular trend from oligotrophic to eutrophic conditions in which the DCM widens and becomes shallower, eventually reaching the surface. This trend can occur in space, for instance by going from the Morocco upwelling to the North Atlantic oligotrophic gyre, or in time, by going from the spring phytoplankton bloom in the North Atlantic to the collapse of the phytoplankton population in summer.

The simplest mathematical representation for this vertical profile is a Gaussian distribution, whose parameters are the depth of the deep chlorophyll maximum, z_m, the standard deviation around the maximum concentration at this peak, and the ratio of the chlorophyll

concentration at depth z_m to total peak biomass (Figure 4-18). Varying these parameters allows any situation, from eutrophic to oligotrophic regimes, to be modeled (e.g., Platt and Herman 1983; Morel and Berthon 1989; Sathyendranath and Platt 1989).

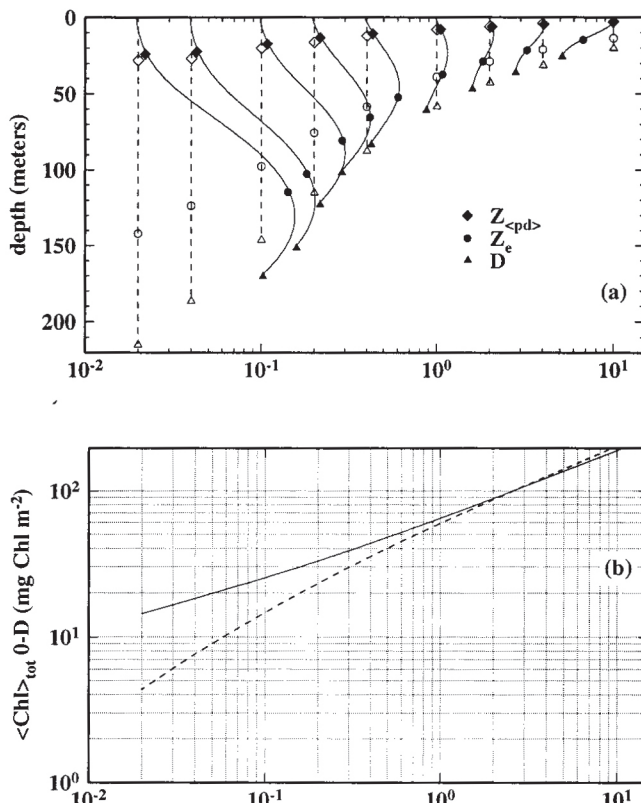


Figure 4-18 Top panel (a): modeled vertical profiles of the chlorophyll concentration as a function of the surface chlorophyll concentration (horizontal axis, units are mg m^{-3})(solid curves; from Morel and Berthon 1989; dashed curve is simply a uniform distribution). " Z_{pd} " is the penetration depth, " Z_e " is the euphotic depth, and "D" is the productive layer (i.e., 1.5 times Z_e). Bottom panel (b): evolution of the total chlorophyll content along with the chlorophyll concentration at the surface. The dashed curve is for homogeneous vertical distributions and the solid curve is for vertically structured profiles, including a deep chlorophyll maximum (DCM). After Figures 1a and 1b in Antoine and Morel 1996.

Water temperature must be similarly extrapolated from satellite observations. Here, the needed parameter is the depth of the mixed layer, within which, by definition, properties are homogeneously distributed. Temperature is constant within the mixed layer, but sharply decreases at the thermocline, and smoothly decreases at greater depths. If the depth of this thermocline is known, a reasonable vertical profile can be reconstructed, from which the mean temperature within the euphotic zone can be derived. The dynamics of the SST might be a clue for gaining insight into the mixed layer (Yan et al. 1991a, b), which, in turn, might be used to infer the depth of this mixed layer. There is no other straightforward way to get information about this depth from remote-sensing observations, and the usual solution is to use either climatology of the mixed-layer depth (Levitus 1982) or outputs from three-dimensional ocean models.

4.4.2 From a Stock, Chlorophyll, to a Flux, Primary Production

Remote sensing is the only avenue for a large-scale estimation of the stock of photosynthesizing algae. Issues related to the extrapolation of surface chlorophyll concentration to a column-integrated value have already been examined. The next step is to determine the amount of carbon that is going through this stock, which determines whether this stock is in a steady state, in a growing phase, or in decay. Here, the transfer function between the stock and the flux has to be determined, i.e., the type of function and the way to parameterize it have to be defined, and the values of the parameters determined.

The function to be defined is the one that relates primary production P for a given phytoplankton biomass B , P^B (units $\text{gC} (\text{gChl})^{-1} \text{s}^{-1}$), to the available light, E (Quanta $\text{m}^{-2} \text{s}^{-1}$). This is the so-called “production versus irradiance” curve, or “ P versus E ” curve. An idealized form of this curve is shown in Figure 4-19, where the irradiance E is expressed either as Photosynthetically Available Radiation, PAR, or as Photosynthetically Usable Radiation, PUR (Morel 1978). P^B_{\max} is the maximum rate and E_k (Talling 1957) is the irradiance where photosynthesis enters into the light-saturated regime. The initial slope of the curve, within the light-limited regime, is generally denoted α^B , and is related to the other parameters through $\alpha^B = P^B_{\max} / E_k$. Various parameterizations have been proposed for this curve (e.g., Steele 1962; Webb 1974; Platt et al. 1980). P versus E curves determined at various depths in the sea from short-time incubation experiments are shown in Figure 4-20, in order to illustrate the great variability that exists in the natural environment as far as α^B , P^B_{\max} , and E_k are concerned. Figure 4-21 also illustrates the vertical repartition of these parameters.

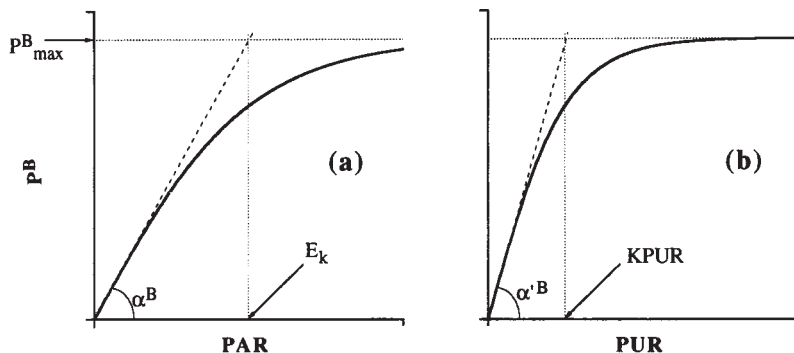


Figure 4-19 Idealized P versus E curve (cf., Table of Symbols), expressed either in terms of the Photosynthetically Available Radiation (PAR, panel a) or the Photosynthetically Usable Radiation (PUR, panel b). Source: Figure 16 in Morel et al. 1996. Reprinted from Morel et al. 1996. Copyright 1996, with permission from Elsevier.

For ocean color remote sensing, the difficulty lies in determining the two parameters, α^B and P^B_{\max} that describe this curve. Note that α^B is related to the quantum yield of photosynthesis, i.e., a quantity that is sometimes measured *in situ*, through the mean absorption coefficient of phytoplankton.

We refer here to the extensive literature on models for determining oceanic primary production, in particular those designed to be fed by remotely sensed observations (e.g., Balch et al. 1989a, b, 1992; Platt et al. 1989; Platt and Sathyendranath 1993). These models usually, if not exclusively, rely on the P versus E curve formalism. Behrenfeld and Falkowski (1997a) give a tentative classification of existing models. Campbell et al. (2002) review the subject and intercompare the response of various models to the same set of *in situ* primary production data.

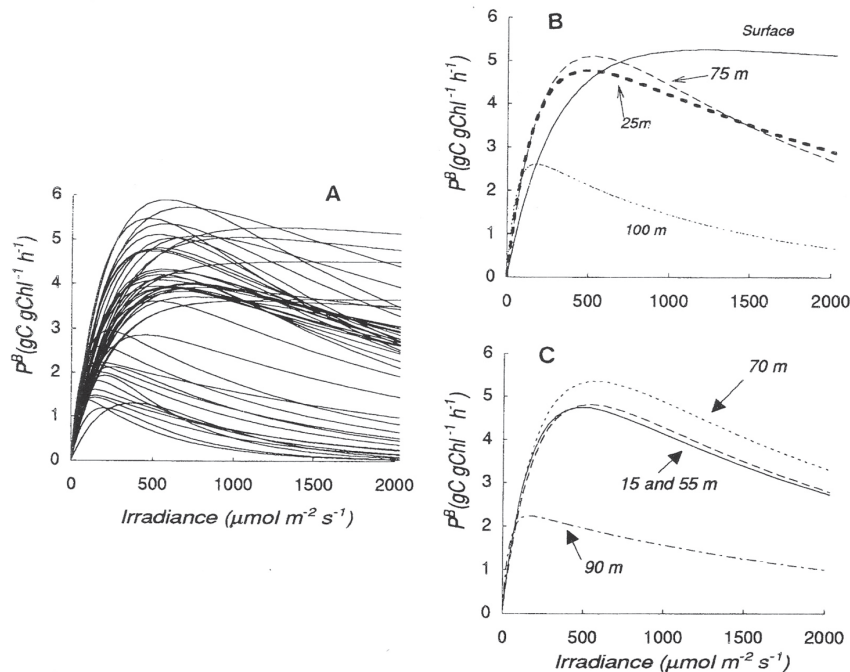


Figure 4-20 Examples of P versus E curves determined from samples collected at various depths. Source: Figure 6 in Cullen et al. 1992. Reproduced with kind permission of Springer Science and Business Media.

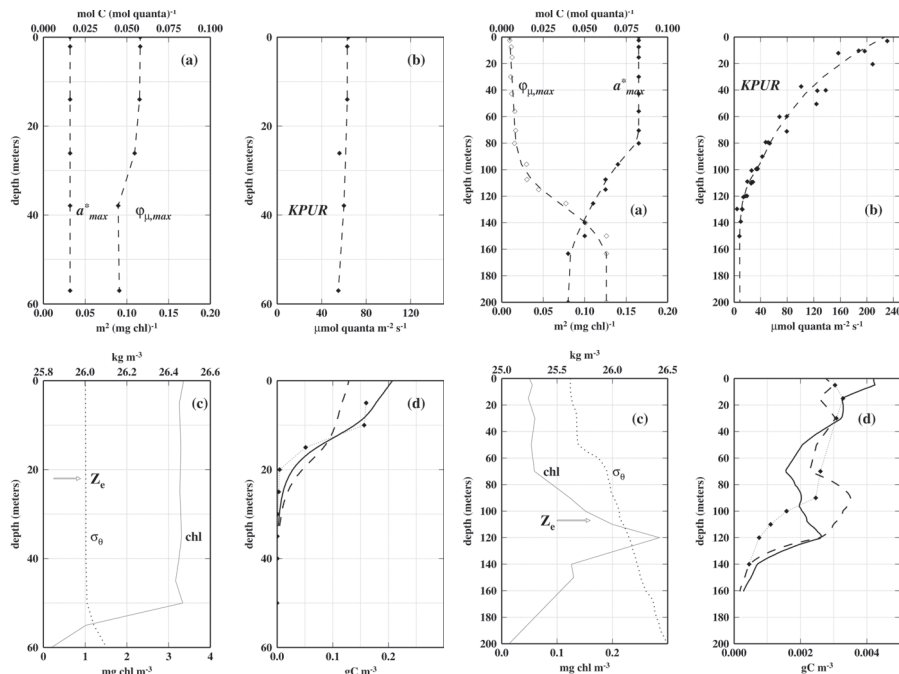


Figure 4-21 Panels (a) and (b): vertical profiles of photo-physiological parameters (cf., Table of Symbols). Panels (c): vertical profiles of the chlorophyll concentration (Chl) and of the water density. Panels (d): vertical profiles of modeled (solid and dashed curves) and measured (diamonds and dotted curve) primary production, as determined at sea in eutrophic (the 4 left panels) and oligotrophic (the 4 right panels) environments (northeast tropical Atlantic). After Figures 6 and 8 in Morel et al. 1996.

4.4.3 From Local Parameterizations and Estimates to Regional or Global Values

Modeling the primary production of a given water-column exposed to a certain amount of irradiation, with a phytoplankton population growing at a specified temperature, essentially provides a unique and local realization of the vertical profile of carbon fixation. The horizontal scale here is the meter; the model is one-dimensional. The situation is similar when performing ^{14}C experiments at sea, with bottles organized along a vertical line containing seawater collected at various depths to which some quantity of radioactive material has been added. The incubation is performed, for instance, during the complete photoperiod, and provides, after integration with respect to depth, a value of the daily, depth-integrated, water-column primary production.

Ideally, remotely sensed measurement of phytoplankton biomass, irradiation and temperature should produce daily estimates of primary production on a pixel basis, which can then be summed over space to provide daily production on the scale of an ocean basin, for instance. Progressively adding the values corresponding to successive days would thereafter lead to weekly, monthly, seasonal and annual estimates. At present, however, the daily coverage of the ocean with ocean color sensors is incomplete (50% of the global ocean with two instruments) (IOCCG 1999). Better coverage is conceivable for restricted areas where cloudiness is low, but even increasing the number of sensors in orbit will never provide full daily coverage of the global ocean, or even of a single oceanic basin such as the Atlantic. An alternative approach, and the most straightforward way to increase the coverage, is to make use of temporal means of the data. For the SeaWiFS instrument for example, 8-day means (composites) are produced, each covering about 50% of the global ocean. Virtually global coverage is obtained with monthly composites.

However, the models derive primary production as non-linear functions of the surface chlorophyll and irradiance, so that use of mean values of these two quantities may cause errors that are hard to predict. We are not aware of a thorough examination of this problem, with quantification of the associated errors (but see IOCCG 2004). A simple example is provided here, which illustrates the type of errors than can be expected (Figure 4-22) when data of different temporal resolutions are introduced into a primary production model.

4.4.4 What Type of Production is Accessible to Space Observations?

Studies (e.g., Platt et al. 1989; Williams 1993), have been made of different types of oceanic production. They vary in the practical way production is measured or modeled, the type of measurement, and the relevant time and space scales. The usual “type” of primary production that is modeled from space observations is the gross production, i.e., the amount of carbon that is fixed by autotrophs, irrespective of the part of this production that is consumed through autotrophic respiration. When the latter is accounted for, the net primary production can be determined and is actually also a result of the modeling in use (even the same model may produce both estimates simply by changing the value of some parameters in the model, such as the quantum yield of carbon fixation). Increasing the complexity of the model might allow one to determine the net community production, which is the net production minus the loss due to respiration by heterotrophs. Determining this quantity in principle requires some knowledge of the food-web structure, which is generally not accessible when using satellite information. These definitions are mostly related to the time scale that is considered, with gross, net, and net community productions corresponding to increasingly longer time scales—typically from minutes and hours (gross), to the photoperiod (net), to one entire day or more (net community). Another separation can be made with respect to the source of nutrient that fuels production; this is succinctly explained below.

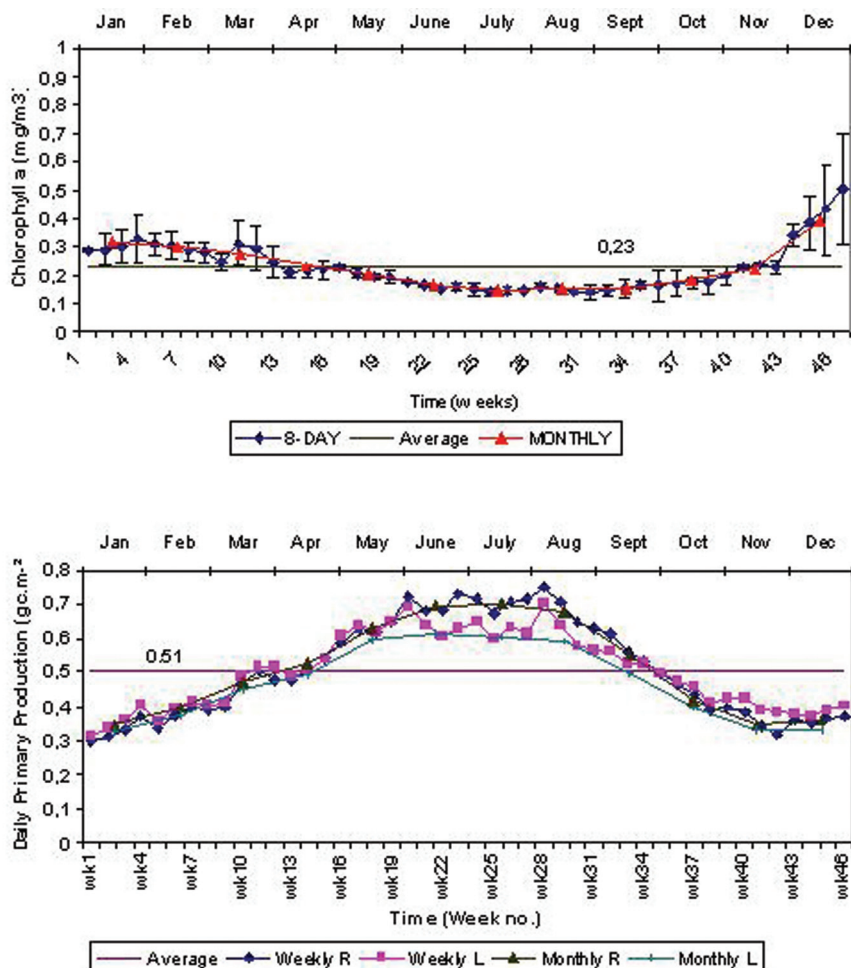


Figure 4-22 Illustration of the differences in the computed primary production (bottom panel), as a function of the temporal resolution of the input chlorophyll fields (top panel: mean Chl evolution), when using either monthly or weekly (actually 8-day) composites of the SeaWiFS observations (Source: Ras 1999). Keywords "L" or "R" relate to the data source that was used for the SST, and stand respectively for Levitus (1982) and Reynolds and Smith (1995). This example is for the entire Mediterranean basin. Courtesy: Joséphine Ras.

The so-called “new” production is highly relevant to present-day concerns about the fate of excess atmospheric CO_2 . If this CO_2 concentration is to be lowered through a change in the efficiency of the biological pump, then new production must be increased, allowing a short-term removal of CO_2 to the deep ocean. The mid- to long-term fate of this carbon is still another issue.

New production was defined (Dugdale and Goering 1967; Eppley and Peterson 1979) as the production realized from “new nutrients,” those brought into the surface layers by physical mechanisms such as upwelling or eddy diffusion, as opposed to the nutrients that are derived from local recycling of organic matter. In a steady state, over some long time scale, this new production must equal the upward flux of nutrients (applying some stoichiometry if production is expressed in terms of carbon). This in turn must equal the downward flux of carbon, also referred to as the “export production.”

New production cannot be estimated directly by remote sensing, but indirect methods can be applied. The most popular technique uses empirical relationships between SST and the concentration of nutrients, then between this concentration and the Eppley “f-ratio” (Eppley and Peterson 1979) (see Figure 4-23), the ratio of new-to-total production. This principle has been applied in upwelling areas, where the local physics essentially drives the nutrient influx, leading to tight relationships between SST and nutrients (e.g., Dugdale et al. 1989; Sathyendranath et al. 1991). The method cannot be applied when physical conditions do not drive the nutrient dynamics, or when these conditions do not have a remotely observable signature. Another disadvantage of this technique is that it closely links new and total production, predicting very similar patterns for both quantities. Although new production may well increase with total production (Eppley and Peterson 1979), this may not hold true for export production, which is the final quantity of interest. The assumption of steady state, although valid over large areas or when considering an entire annual cycle locally, may become irrelevant when computing new production at a given station and for a given day. This is exactly the situation in which production algorithms are applied to remote sensing observations.

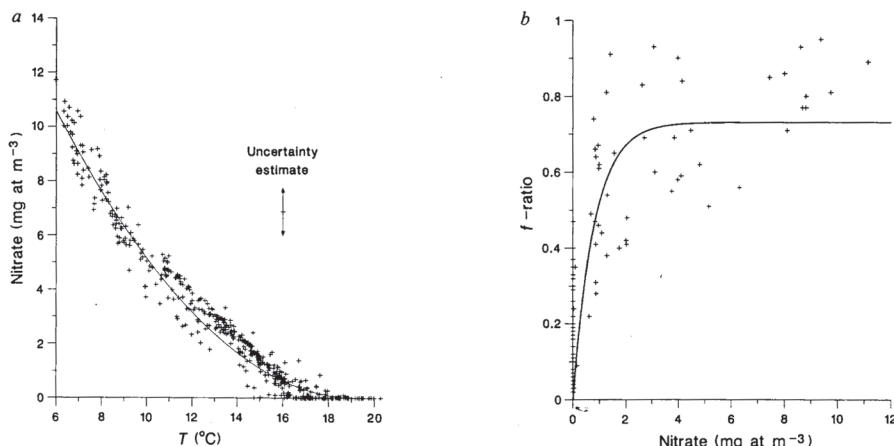


Figure 4-23 Left panel: relationships between nutrients (nitrate) and the sea surface temperature (SST). Right panel: relationships between the nitrate concentration and the f-ratio. Source: Figure 3 in Sathyendranath et al. 1991.

A different technique has been recently proposed to derive new production. It uses radar altimetry (Turk et al. 2001) that is supposed to provide the depth of the nutricline, which in turn is empirically related to new production.

4.5 GLOBAL DISTRIBUTION OF PARAMETERS DETERMINING PRIMARY PRODUCTION AND ITS MODELING FROM SPACE OBSERVATIONS

In this section, we describe the global distributions of quantities that determine oceanic primary production, as remotely observed from space, before looking into the primary production itself (Section 4.6). The first maps of global primary production in the world ocean mostly were derived from distributions of its governing factors (Ryther 1969; Koblentz-Mishke et al. 1970). Accurate assessments of the incoming solar flux and the integrated biomass can be sufficient to give acceptably correct values for the global primary production.

4.5.1 Phytoplankton

Figure 4-24 shows the distribution of phytoplankton in the world ocean for the four seasons. The major features are related to the general circulation of the water masses and to local phenomena such as upwellings and fronts, which are the driving forces for the transport of nutrients towards the upper layers. Phytoplankton will grow when light and nutrients are both available, except where vertical mixing is too intense or a particular chemical element is lacking (see Sections 4.5.3 and 4.5.5).

The regions of lowest chlorophyll concentration (the “oligotrophic” areas; purple color on the map) are essentially located within the subtropical gyres, where solar illumination is high and waters are stratified throughout the year. Most seasonality in these regions is related to the variation in the incoming solar flux, rather than to significant changes in the physics and water circulation. Permanent stratification prevents significant amounts of nutrients being brought to the upper lit layers, limiting biomass growth. The southeastern Pacific gyre is definitely the most oligotrophic area of the world ocean according to Figure 4-24. Surprisingly, this “biological desert” is little studied. It may reveal interesting and specific features, for instance in terms of optical properties and phytoplankton populations.

At the other extreme are the “eutrophic areas” (say, where chlorophyll concentration is above 1 mg m^{-3} , i.e., starting with the yellow color on Figure 4-24), which can be the result of a variety of environmental factors that drive nutrients toward the surface. Coastal upwellings (off Senegal, Peru, and Namibia), oceanic fronts (Agulhas current area), regions of high horizontal dynamics including eddies (Gulf Stream, north Pacific Kuroshio current), and also strong wind or convective mixing are the major processes allowing intense phytoplankton growth in the open ocean. The same phenomena, but of lower strength, are also driving growth in mesotrophic areas, i.e., these areas where the concentrations are moderate (between 0.1 and 0.5 mg m^{-3}). A special situation exists, however, where the relatively high nutrient concentrations maintained by these physical mechanisms are not fully used, so that the phytoplankton populations remain at a moderate level (usually below 0.2 mg m^{-3}). These areas are the “High Nutrient Low Chlorophyll” (HNLC) areas, the largest being the southern ocean south of the Antarctic convergence, the eastern equatorial Pacific and the northeast (sub-arctic) Pacific.

Nearer to continents, river outputs, tidal mixing, and resuspension of bottom sediments are other mechanisms that significantly and transiently increase the nutrient concentrations, allowing phytoplankton to bloom. These regions, along with the coastal upwellings, produce the vast majority of the world fish catch. Global distributions and temporal evolutions have been described by Yoder et al. (1993).

4.5.2 Available Radiant Energy

Figure 4-25 shows the varying amount of radiant energy available at the sea surface for the four seasons, which is then available for photosynthesis. Obviously this distribution is primarily driven by the inclination of the Earth’s axis, with maxima moving across the equator with the seasons. The cloud distribution is superimposed on this annual pattern, which generates a complex and patchy distribution that would be even patchier when considered on a daily scale. At high latitudes, abundant phytoplankton populations remain in darkness during a significant portion of the year. The highest levels are in the inter-tropical band, and a relative minimum occurs near the equator in the Pacific, due to the permanent cloudiness there.

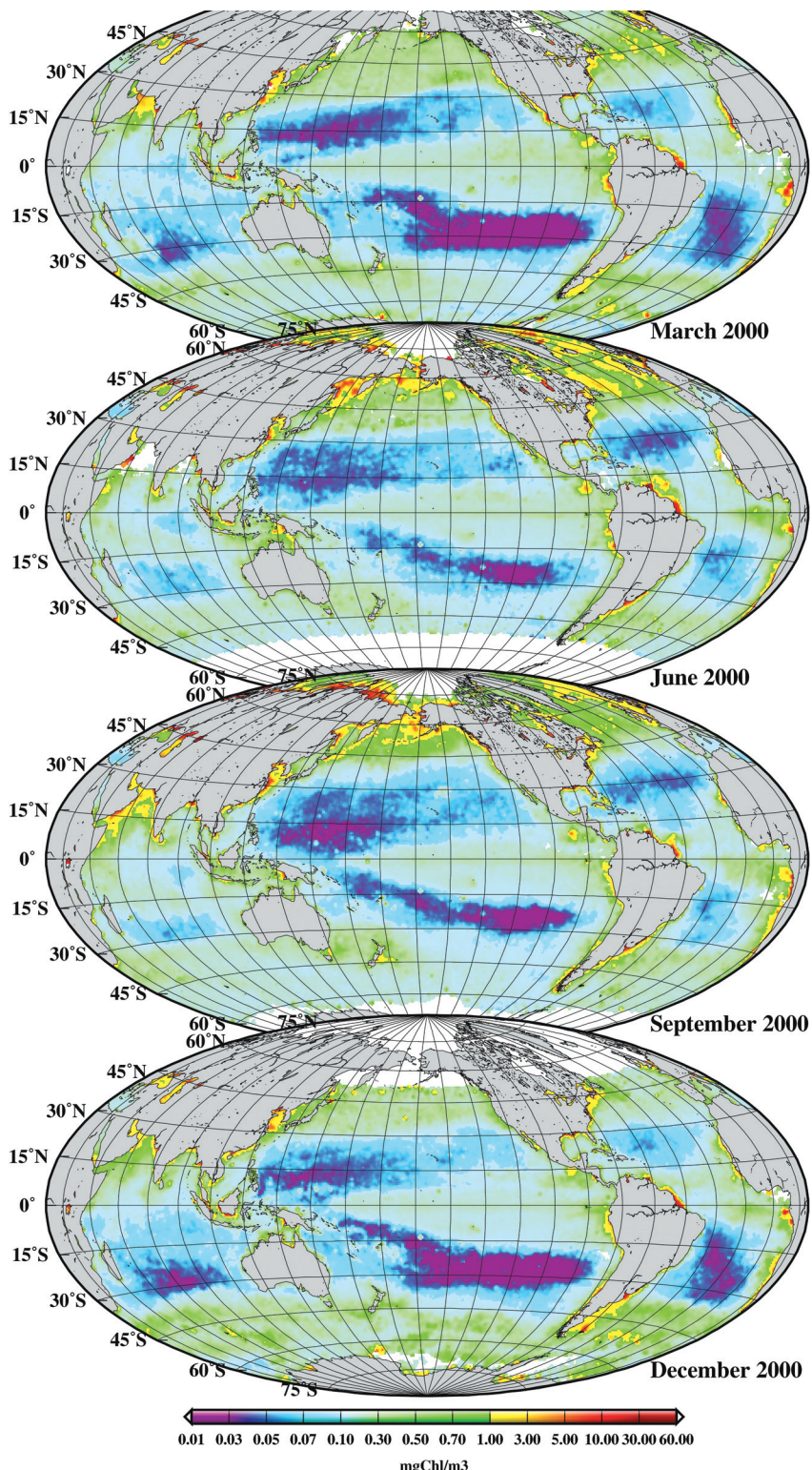


Figure 4-24 Global maps of chlorophyll distribution derived from the SeaWiFS observations for the four months indicated. Data obtained from the NASA Goddard Space Flight Center (GSFC) Distributed Active Archive Center (DAAC).

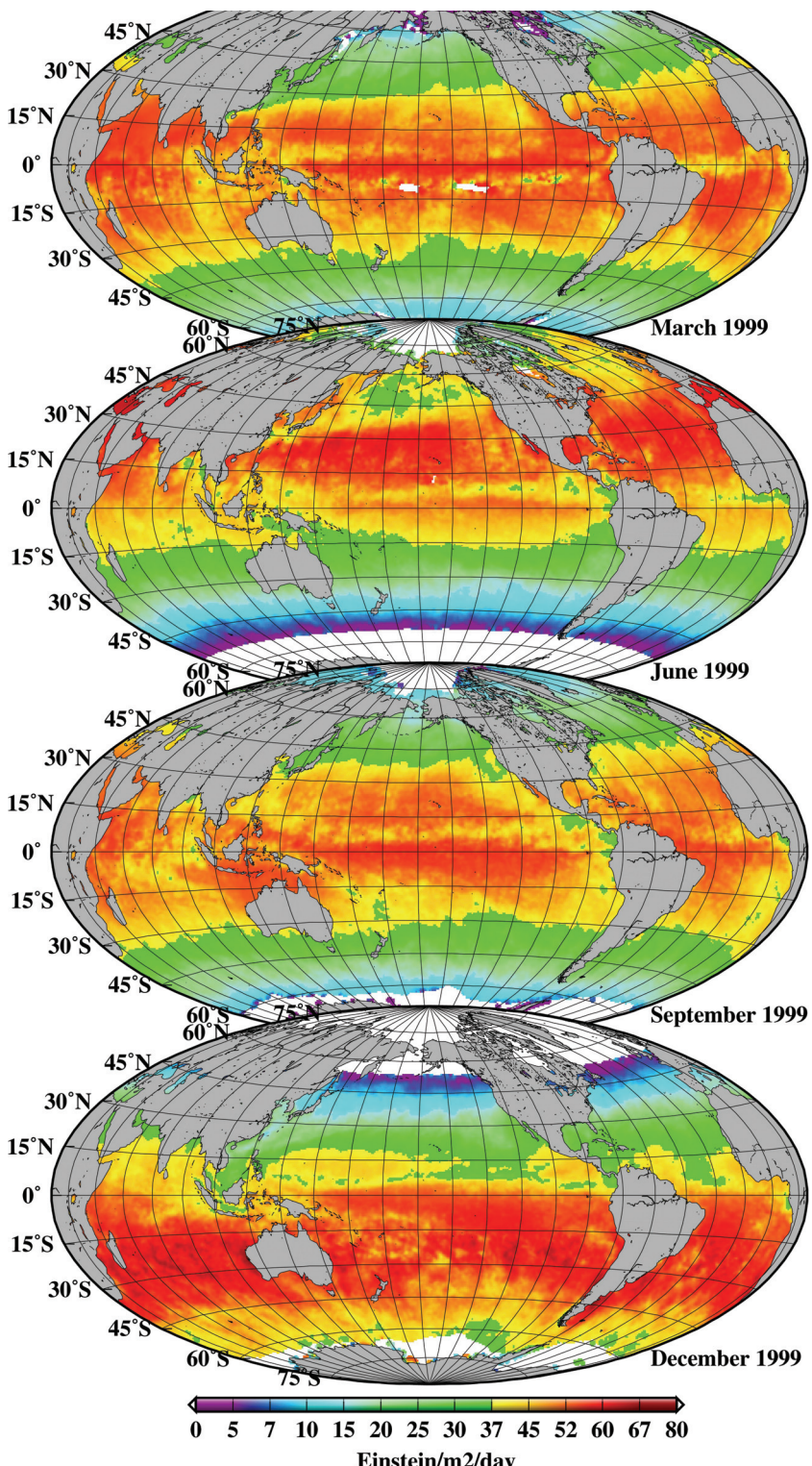


Figure 4-25 Global maps of the "Photosynthetically Available Radiation" (PAR) incoming at the sea surface, as derived from SeaWiFS observations and the Frouin et al. (2003) modeling. Data obtained from the NASA Goddard Space Flight Center (GSFC) Distributed Active Archive Center (DAAC).

This global view does not consider the daily changes in cloudiness that occur in any given area; cloudiness affects the daily amount of radiant energy and its distribution during the day. This is one important aspect of modeling primary production that cannot be tackled using remote-sensing data, however, because the best temporal resolution attainable is on a daily basis (at least when using only polar-orbiting satellites).

For a given mean cloudiness, the combination of the changes over a day in the photo-physiological status of phytoplankton and of the changes of cloudiness (constant, patchy, over one half of the day only, etc.) may lead to different answers in terms of the daily primary production.

4.5.3 Sea Surface Temperature, Vertical Mixing

The global distribution of sea surface temperature is shown in Figure 4-26, again for the four seasons. Large-scale features due to local physical forcing, such as the upwellings (off West Africa and Peru), appear in these maps. Some noticeable features are the permanently cold waters of the southern ocean, the large pool of warm waters in the western equatorial Pacific (the “warm pool”), and the tongue of cold waters along the equator in the Pacific, due to local upwelling in this area. These cold waters disappear during El Niño events, when the waters from the warm pool invade the equatorial Pacific (McPhaden 1999; Chavez et al. 1999). When looking at the whole range of ocean temperatures, at its seasonal variations, and at its significant inter-annual changes, one immediately understands that the modeling of the temperature effect on photosynthesis is particularly important in accurately assessing the global carbon fixation and its regional distribution.

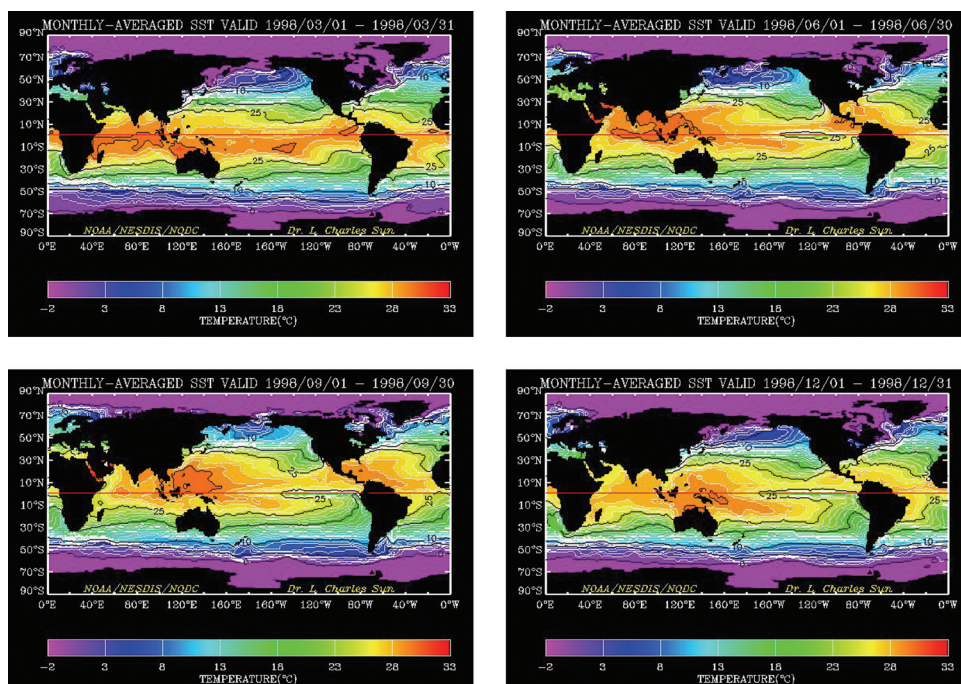


Figure 4-26 Global seasonal maps of sea surface temperature, as derived from AVHRR observations. Source: <http://www.nodc.noaa.gov/dsdt/oisst/monthly/gif/199803.gif & 199806.gif & 199809.gif & 199812.gif>. Courtesy: NOAA National Oceanographic Data Center.

When modeling photosynthesis, the vertical temperature profile is required, not just the surface value, and a relationship between temperature and the maximum rate of photosynthesis would be deduced from this profile in order to get P^B_{\max} at each depth. Climatologies or model outputs can be used to give a correct value of the mean temperature within either the mixed layer or the euphotic layer, depending on the ratio between both. The depth of the euphotic layer can be derived from the surface chlorophyll concentration (e.g., Morel and Berthon 1989), and information about the vertical structure of the water column is derivable from mixed-layer depths so that a mean temperature can be derived (e.g., Bricaud et al. 2002); this is relevant for calculating P^B_{\max} . This value may be inadequate for deeper layers, yet at these depths photosynthesis is no longer light-limited so that the exact knowledge of P^B_{\max} is not required.

4.5.4 Nutrients

Once the physical environment of phytoplankton is described (radiant energy, temperature, mixing), the nutrient availability must be known as well, in order to get a comprehensive picture of what potential carbon fixation is possible. Figure 4-27 shows for instance a global climatological map of the nitrate concentration in the upper ocean layer (data from Levitus 1982). If river inputs are not considered, the distribution is entirely determined by the three-dimensional dynamics of the ocean, which ensures a regular refueling of the upper layers either from deep waters (coastal and equatorial upwellings) or from adjacent waters (horizontal advection of water masses).

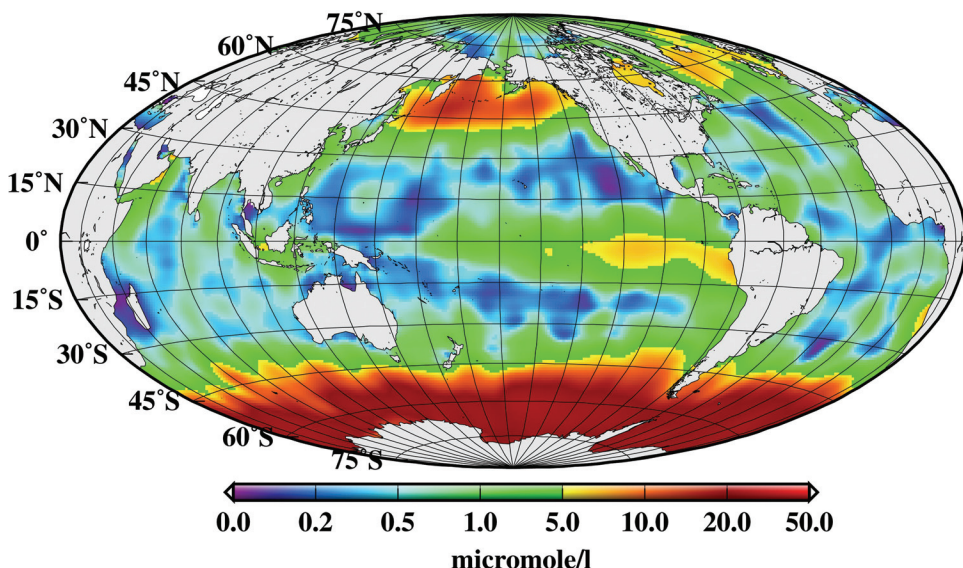


Figure 4-27 Distribution of nitrates in the world ocean surface layer, using data from Levitus 1982.

This important information is presently not derived from any source of remote-sensing observations. A possibility exists to indirectly achieve this goal from radar altimeter measurements that are providing information about the upper ocean dynamics and, in turn, can help in determining the nutrient inputs to the upper ocean.

4.5.5 Other Elements

Atmospheric input of nutrients or of minor elements is suspected to be a significant driving force leading to the present pattern of phytoplankton production in the world ocean (e.g., Duce et al. 1991; Martin et al. 1994). One possible explanation of the “High Nutrient Low Chlorophyll” areas mentioned in Section 4.5.1 would be the lack of certain key oligo-elements such as iron, preventing an efficient use of the nutrients present in the water column. The map shown in Figure 4-28 illustrates the large regional differences in the input of iron from land to the oceans, as carried by aerosols extracted from dry areas such as the Sahara. There is considerable colocation of oligotrophic areas with areas of minimum atmospheric deposition, yet no causal relationship has yet been demonstrated.

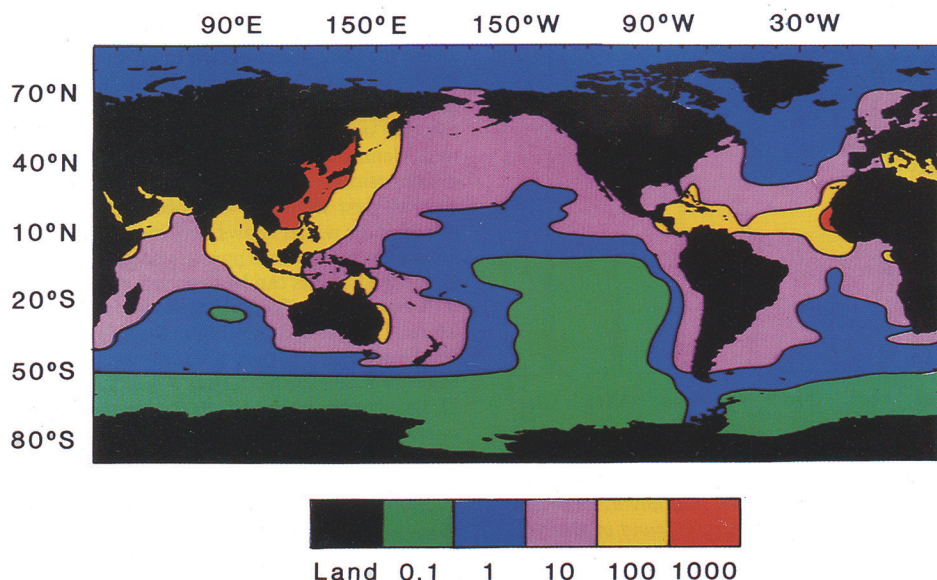


Figure 4-28 Atmospheric-deposition flux of total iron to the ocean ($\text{mmol m}^{-2} \text{ yr}^{-1}$). Source: Figure 1 in Donaghay et al. 1991, from data given in Duce et al. 1991.

Significantly changing this pattern by increasing the area of dry surface over land, for instance, might lead to a change in the deposition pattern of iron and other elements such as phosphorus, and ultimately to a change in the global distribution of primary production. It is now conceivable that maps such as the one shown here (Figure 4-28) could be derived routinely from satellite observations using ocean color to map aerosol types and amounts (optical thickness) above the ocean. It remains to be determined whether or not these micronutrient inputs have a global impact as compared to the main nutrient inputs from deep waters (Section 4.5.4).

4.6 GLOBAL PRIMARY PRODUCTION ESTIMATES FROM REMOTE SENSING OBSERVATIONS

Various models have been developed in the past decades to derive primary production from space observations. The examples provided below illustrate the variety of approaches that are possible, even when the basic data sets in use are similar and even identical, as is the

case here for Sections 4.6.1, 4.6.2 and 4.6.3, with the exception of a few details. Indeed, these three works used the same climatology for ocean color (CZCS) and sea surface temperature (SST) when relevant (Levitus 1982), and very similar data sets for estimating the surface irradiation. Differences are in the “transfer function” (i.e., how to go from a stock to a flux) and the parameters attached to it.

The works considered here illustrate different ways of tackling the problem. They converge on extremely close values for the global primary production, while they may significantly diverge locally. This observation may suggest that global numbers are rather insensitive to the exact way they have been obtained, simply because they are heavily constrained by inescapable physical principles and the global integrated energy available. A precise estimation of the latter would be therefore the key for successful global estimates, rather than improved and more detailed modeling. This is precisely where remote sensing brings its unique contribution.

These works can be considered as the achievements of large-scale ocean primary production modeling in the 1990s. They are all partly demonstration studies as well as true quantitative assessments of this critical flux. The next step is to go from these “academic” exercises towards a true monitoring of the year-to-year and decadal changes in the oceanic primary production. This will require the availability in the future of consistent, long-term, satellite ocean-color records (Gregg and Conkright 2002; Gregg et al. 2003; Antoine et al. 2005), as well as a lot of work in the field of phytoplankton photo-physiology and its relation to environmental factors.

4.6.1 Longhurst, Sathyendranath, Platt, and Caverhill 1995

The specificity of the work by Longhurst and co-workers (Longhurst et al. 1995; hereafter referred to as L95) is to be found in the partitioning of the ocean into biogeochemical domains and provinces. When globally considering the ocean, there is by definition a compelling need to cope with the whole range of variability in all parameters involved in the modeling of primary production. The solution adopted in L95 consists in pooling together a sufficiently large number of *in situ* observations so that mean parameters can be derived for domains (subdivided into provinces), which have been delineated from *a priori* oceanographic knowledge. These domains separately consider the polar regions, the oligotrophic gyres in each ocean, or the coastal upwellings. Details and specific arguments on this delineation can be found in Longhurst (1995). In the work by L95 seasonal changes within provinces are not considered. This could be added as soon as enough data are collected to define the annual cycle of parameters.

The parameters for which mean values are computed over these domains are the two descriptors of the “ P^B versus E” curve and the parameters describing the shape of the vertical distribution of chlorophyll in the upper layers. For the “ P^B versus E” curve, they are α^B , the initial slope of the curve, and P^B_{\max} , the value of the plateau reached for high irradiances (formerly referred to as the “assimilation number”). For the biomass distribution, they are the depth of the deep chlorophyll maximum, z_m (which tend to zero, i.e., towards the surface, when the chlorophyll concentration is high, and deepens when shifting to oligotrophic regimes), the standard deviation around the maximum concentration at this peak, and the ratio of the chlorophyll concentration at depth z_m to total peak biomass. These parameters actually determine the shape of a Gaussian curve, whose peak mimics the DCM.

The information about parameters was introduced into the modeling described in Sathyendranath et al. (1995), which also took as inputs the CZCS climatology (Feldman et al. 1989) and the cloud-cover climatology of Hahn et al. (1987) for calculating available

irradiation at the sea surface. The resulting primary production map is shown on Figure 4-29a, which leads to integrated global annual productions between 40.7 and 50.2 Gt C, depending on the assumption made about the error in Case 2 coastal waters (in these waters the chlorophyll concentration derived from ocean color observations essentially is overestimated, by at least a factor of 2).

In L95, the authors advocate defining biogeochemical provinces using the large differences in regional primary production estimates, mostly due to differing selections of parameters. The acknowledged limitation of this approach is the lack of flexibility and the need for continued revision of the mean values assigned to the provinces when assessment of the long-term evolution of oceanic primary production is the aim. This would mean continuing additional measurements at sea.

4.6.2 Antoine, André, and Morel 1996

Morel and Berthon (1989) and Antoine and Morel (1996) made use of an equation that estimated primary production from the photosynthetically available radiation impinging at the sea surface, $\text{PAR}(0^+)$ ($\text{J m}^{-2} \text{ t}^{-1}$), the chlorophyll content of the water column, $\langle \text{Chl} \rangle_{\text{tot}}$ (mgChl m^{-2}), and the cross section for photosynthesis per unit of areal chlorophyll, Ψ^* ($\text{m}^2 \text{ mgChl}^{-1}$).

$$P = (1/39) \text{PAR}(0^+) \langle \text{Chl} \rangle_{\text{tot}} \Psi^* \quad (4-24)$$

This requires determining a “climatological field” of the Ψ^* quantity. Ψ^* depends on the two other terms of the equation ($\text{PAR}(0^+)$ and $\langle \text{Chl} \rangle_{\text{tot}}$) and on temperature. Therefore such a “climatological field” is conveniently represented by look-up tables; the entries are date, latitude, cloudiness, temperature, and remotely sensed chlorophyll concentration. These tables are produced by using a previously published spectral light-photosynthesis model (Morel 1991a), which necessarily relies on a standard set of ecological and photo-physiological parameters. The method proposed (Antoine and Morel 1996) can accommodate any improvement and complexity in parameterizations (e.g., Morel et al. 1996), to the extent that additional computation is only needed when generating the Ψ^* tables, not when using these tables in conjunction with satellite data. This method has been used for several studies, at both regional (Morel and André 1991; Antoine et al. 1995) and global (Antoine et al. 1996) scales.

The solution adopted to cope with the difficulty of reconstructing the vertical biomass distribution is somewhat different from that of Longhurst et al. (1995). The vertical distribution is also represented by a Gaussian curve, but determination of the parameters (position, intensity and width of the peak, and value of the background) is through smooth relationships between these parameters and the surface chlorophyll concentration. These relationships were obtained by a statistical analysis of thousands of vertical biomass profiles, distributed in various oceanic regimes (Morel and Berthon 1989). The underlying idea is that a continuum exists between oligotrophic and eutrophic situations, with the surface chlorophyll concentration indicating the trophic regime. Exceptions inevitably exist, but the statistical representation is valid in many circumstances. In addition, it has been shown that a precise determination of the vertical biomass distribution is not so important when global values are the aim (Antoine et al. 1996). The picture is more variable when looking at individual, local predictions of the model. The resulting global map is shown in Figure 4-29b, and the corresponding global value is 46 GtC per year.

4.6.3 Behrenfeld and Falkowski 1997

To a certain extent, the work by Behrenfeld and Falkowski (1997b), hereafter referred to as BF97, is similar to that of Longhurst et al. (1995), because it relies on *in situ* observation. In BF97, several thousands of vertical profiles of primary production, as determined from ^{14}C incubations, were pooled together and normalized with respect to chlorophyll concentration at each depth, photoperiod (i.e., day length), and optical depth. A consistent pattern emerged for the vertical distribution of primary production and was the basis of what they called the “Vertically Generalized Production Model” (VGPM). This “resembles a suite of empirical relationships” (BF97) from which primary production is estimated from the local chlorophyll concentration, the day length, the depth of the euphotic layer, the available irradiation at the sea surface, and the P^B_{opt} parameter. The latter parameter is the “maximum carbon fixation rate within the water column,” i.e., the maximum of the vertical primary production profile when normalized as described above. The value of P^B_{opt} (which is different from the P^B_{max} parameter) was parameterized as a function of the temperature using a seventh order polynomial, which gave a simple access to its value when working from satellite observations at large scale. Because this model is a purely empirical one, its applicability “outside” of the spatial or time domain where it was developed could be challenged, though that domain covered a large portion of the global ocean and several years.

In this model, the vertical resolution is implicitly accounted for through the use of the large database of *in situ* determinations of primary production. The resulting annual global primary production obtained when this model is applied to the SeaWiFS observations is of about 45 GtC, as shown in Figure 4-29c. The same method has been used in conjunction with land primary-production models in order to provide a global view of the autotrophic carbon fixation on Earth (Field et al. 1998).

4.7 CONCLUSIONS, PERSPECTIVES

4.7.1 Global Production and Its Long-term Changes

Although very significant results have been obtained, as discussed in Section 4.6, significant difficulties remain in improving the estimate of oceanic primary production and in predicting its changes with any variation of “oceanic climate” (increase in temperature, change of nitrate supply, etc.). Studies have so far been demonstrations of feasibility, using climatologies for chlorophyll, temperature and cloud cover, as well as constant parameters to describe the photosynthetic function. This explains partly why no significant revisions have appeared with regard to the production of the world ocean since the three works summarized in Section 4.6, even though ocean color satellite data has been rapidly accumulating since the launch of several sensors, starting with POLDER and OCTS in 1996, SeaWiFS in 1997, MODIS in 1999 and 2002, and MERIS in 2002. More recent papers on the topic do bring innovative concepts (e.g., Behrenfeld et al. 2001); they use more recent data for Chl (SeaWiFS data), SST (Reynolds analyses) or PAR (also SeaWiFS data). The modelling itself has made relatively little progress, and the estimates of the total primary production remain about the same, around 50 gigatons of carbon per year (see for example Morel and Antoine 2002).

The current difficulty is not in the accuracy of this figure, but rather in our capacity to study the interannual and decadal changes of production. The average total value is strongly determined by the radiative energy and the phytoplankton biomass at the scale of the world

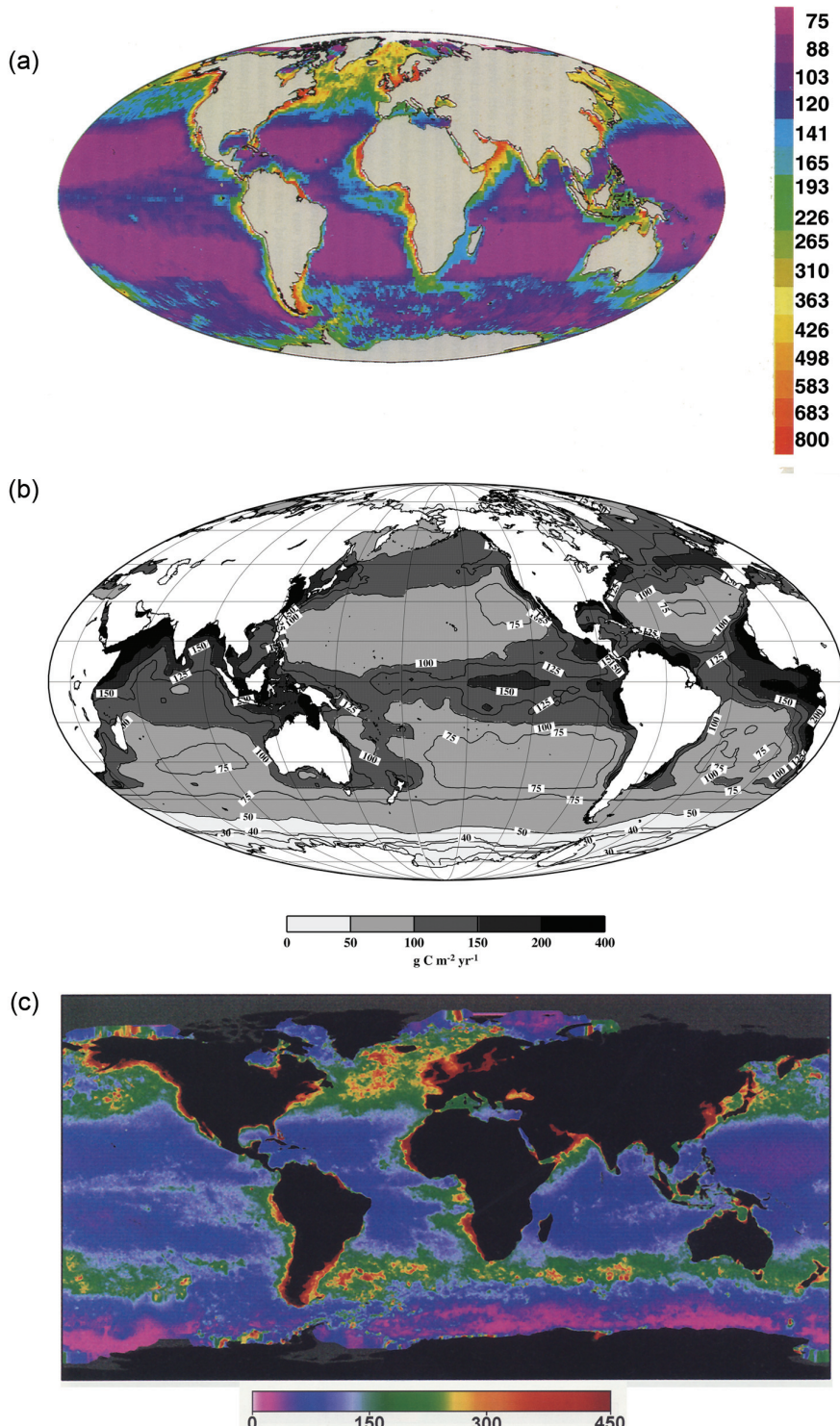


Figure 4-29 Three global maps of the annual primary production determined from CZCS observations ($\text{gC m}^{-2} \text{ yr}^{-1}$). Panel (a): Source: Figure 3 in Longhurst et al. 1995, courtesy: Oxford University Press. Panel (b): Source: Figure 3 in Antoine et al. 1996. Panel (c): Source: Figure 9A in Behrenfeld and Falkowski 1997b. Copyright 1997 by the American Society of Limnology and Oceanography, Inc.

ocean, both rather well determined, and by the average capacity of the phytoplankton to use this energy, which is much less certain. The study of temporal variations implies moreover that all the necessary data (at least chlorophyll, temperature and illumination) are derived with the required accuracy and stability over long periods of time (decades). One of the prime motivations for launching a variety of ocean color instruments aboard satellite platforms is to be able to build such a long-term archive. This will then allow us to identify possible changes in the state of the oceanic biomass, in response to basin-scale or global environmental change. The present global carbon budget (over the last century) is not in balance, as is shown by continuous recording of atmospheric CO₂ performed at the Mauna Loa Observatory in Hawaii and in many other places around the planet. This increase actually reflects the incomplete transfer of carbon dioxide, produced by burning of fossil fuels, into marine and terrestrial biomass. Whether or not the oceanic phytoplankton can incorporate this excess CO₂ is presently unknown. The answer is probably not reachable without the help of remote sensing techniques. Difficulties along the way are multiple, first because we do not have a long record of global ocean color. Modern ocean color sensors were launched in 1996 and 1997. The pioneering observations made by the Coastal Zone Color Scanner mission (1979 to 1986) are, however, a possible starting point for building this long-term record. It is one of the reasons that several groups engaged in the construction of long-term ocean color satellite archives (Gregg and Conkright 2002; Gregg et al. 2003; Antoine et al. 2005).

4.7.2 Uncertainties in Algal Photo-physiology

It is also necessary that primary production models include parameterizations allowing changes in photosynthetic efficiency to be accounted for, in response to variations in environmental conditions. This is not possible at the present time. Improvements have been made in modelling light propagation and its availability for photosynthesis, whereas large uncertainties remain in phytoplankton photo-physiology. Research to be undertaken relates in particular to the effect of temperature and nutrient levels on photosynthetic carbon fixation, in particular on the maximum rate of photosynthesis per unit of biomass (P^B_{max}), and on relating parameters describing these processes to parameters easily accessible to satellite observations, in particular temperature and radiation. Possible progress, or at least a detailed state of the art, is at reach through inter-comparison of models (Campbell et al. 2002; Carr et al. 2005). This can lead to identification of problems and of remaining weaknesses, so that critical research areas can be identified.

With regard to the effect of temperature on P^B_{max}, no solution emerges for the moment. Indeed, without entering into details, there are various parameterizations of the changes of P^B_{max} with temperature (e.g., Eppley 1972; Behrenfeld et al. 1997b). The difficulty on the one hand is that none of these parameterizations, which give appreciably different results, can be selected on objective criteria as being better than another, and, on the other hand, that they are all derived according to the same type of laboratory experiment whose results are hardly transferable to the oceanic environment. These experiments consist in applying rather large temperature variations to natural populations or cultures and deducing from their response some laws of variations for the growth rate according to the temperature. The imposed temperature changes do not correspond in general to the changes that algal populations actually meet in their natural environment, and the application of these relationships is thus hazardous. The solution is undoubtedly not in the repetition of these types of experiments (unless their protocol is appreciably altered), but perhaps rather in the acquisition of additional data in various areas of the ocean. These data can contribute to the understanding

of mechanisms responsible for changes in photosynthetic parameters and can also feed the databases necessary for definition of biogeochemical provinces (Longhurst 1995). At the moment, the various parameterizations of the effect of temperature on P_{\max}^B are being more frequently challenged. Instead, work is concentrating on environmental determination of P_{\max}^B through phytoplankton assemblages and nutrient availability (e.g., Behrenfeld et al. 2002).

4.7.3 New Approaches

Methods that have been developed in the past decade to estimate oceanic primary production from satellite observations are essentially based on the same principles, and mostly differ in their level of complexity (Behrenfeld and Falkowski 1997a). The basic idea is to model the transfer function between a stock of carbon (phytoplankton biomass) and the flux of carbon transiting this pool (primary production). It is uncertain whether the flux can be observed and quantified directly, except perhaps when estimating new production from altimetry measurements (Turk et al. 2001).

The contours of a new approach are progressively appearing by monitoring the daily cycle of the particle load of surface waters, which is a good proxy for primary production (Claustre et al. 1999). This could become possible in the relatively near future with the renewed interest in geostationary satellites, onto which it is now feasible to install ocean color sensors equipped with the relevant spectral bands and with sufficient radiometric accuracy. Observations of the full Earth disk are within reach from such platforms, and at a temporal resolution of one hour or less. It may be, therefore, that we will quite soon have the ability to track the particle load on a very fine time scale, allowing a near-real-time and direct assessment of oceanic primary production at basin-scale (Behrenfeld et al. 2005).

Table of Symbols

Subscripts used for various coefficients:

w	Pure sea water
ϕ or ph	Phytoplankton
p	Total particles
nap	Non-algal particles
ds	Dissolved substances
a	Aerosol scattering
r	Rayleigh scattering

Geometry, general:

λ	Wavelength	nm
θ_s	Solar zenith angle (cosine is μ_s)	degrees
θ_0	Solar zenith angle (cosine is μ_0)	degrees
θ_v	Satellite viewing angle (cosine is μ_v)	degrees
θ	Satellite viewing angle (cosine is μ)	degrees
θ'	$\theta' = \sin^{-1}(\sin(\theta_v) / 1.34)$	degrees
$\Delta\phi$	Relative azimuth difference angle	degrees

Inherent optical properties:

a	Absorption coefficient	m^{-1}
a^*	Specific absorption coefficient	$m^2 g^{-1}$
	Absorption coefficient per unit of concentration	
$\beta(\theta)$	Volume-scattering function (VSF)	$m^{-1} sr^{-1}$
$\beta(\theta)$	Normalized VSF: $\beta(\theta)/b$	sr^{-1}
b	Total scattering coefficient	m^{-1}

$$\text{with } b = 2\pi \int_0^\pi \beta(\theta) \sin(\theta) d\theta$$

b^*	Specific scattering coefficient	$m^2 g^{-1}$
	Scattering coefficient per unit of concentration	
b_b	Backscattering coefficient	m^{-1}
	Integration of $\beta(\theta)$ from $\pi/2$ to π	
\tilde{b}_b	Backscattering probability, i.e., b_b/b	
c	Attenuation coefficient ($c = a + b$)	m^{-1}
η	Ratio of water scattering to total scattering : b_w/b	
η_b	Ratio of water backscattering to total backscattering : b_{bw}/b_b	
n	Refractive index	
ω	Single-scattering albedo : $\omega = b / c$	

Other quantities:

Chl	Chlorophyll concentration	$g(Chl) m^{-3}$
E_d, E_u	Downwelling and upwelling irradiances : Integration of radiances over the two hemispheres	$W m^{-2}$

$E_d = \int_0^{2\pi} \int_0^{\pi/2} L(\theta, \phi) \sin(\theta) \cos(\theta) d\theta d\phi ,$		
$E_u = \int_0^{2\pi} \int_{\pi/2}^{\pi} L(\theta, \phi) \sin(\theta) \cos(\theta) d\theta d\phi$		
$E_d(0^+)$	Downwelling irradiance just above the sea surface	W m^{-2}
$E_d(0^+) = \epsilon_e F_0 \mu_0 T$, where ϵ_e is a function of the eccentricity of the Earth orbit and T the atmospheric transmittance		
$E_d(0^-)$	Downwelling irradiance just below the sea surface	W m^{-2}
ϵ	Coefficient of the spectral dependence of the aerosol radiance	dimensionless
f or $F_{L' \beta}$	Coefficient relating R to the inherent optical properties	
F_0	Extraterrestrial solar irradiance	$\text{W m}^{-2} \text{ sr}^{-1}$
F'_0	F_0 reduced by two trips into the atmosphere	$\text{W m}^{-2} \text{ sr}^{-1}$
K_d	Diffuse attenuation coefficient for the downwelling irradiance	m^{-1}
$L_t(\lambda, \theta_s, \theta', \Delta\phi)$	Total radiance at the top of the atmosphere	$\text{W m}^{-2} \text{ sr}^{-1} \mu^{-1}$
$L_r(\lambda, \theta_s, \theta', \Delta\phi)$	Radiance due to Rayleigh scattering	$\text{W m}^{-2} \text{ sr}^{-1} \mu^{-1}$
$L_a(\lambda, \theta_s, \theta', \Delta\phi)$	Radiance due to aerosol scattering	$\text{W m}^{-2} \text{ sr}^{-1} \mu^{-1}$
$L_{ra}(\lambda, \theta_s, \theta', \Delta\phi)$	Radiance due to aerosol-molecule scattering interactions	$\text{W m}^{-2} \text{ sr}^{-1} \mu^{-1}$
$L_{as}(\lambda, \theta_s, \theta', \Delta\phi)$	Radiance due to aerosol scattering, in the single-scattering approximation	$\text{W m}^{-2} \text{ sr}^{-1} \mu^{-1}$
$L_g(\lambda, \theta_s, \theta', \Delta\phi)$	Radiance due to sun glint	$\text{W m}^{-2} \text{ sr}^{-1} \mu^{-1}$
$L_f(\lambda, \theta_s, \theta', \Delta\phi)$	Radiance due to the presence of foam at the sea surface	$\text{W m}^{-2} \text{ sr}^{-1} \mu^{-1}$
$L_w(\lambda, \theta_s, \theta', \Delta\phi)$	Water-leaving radiance	$\text{W m}^{-2} \text{ sr}^{-1} \mu^{-1}$
$[L_w]_N(\lambda, \theta_s, \theta', \Delta\phi)$	Normalized water-leaving radiance	$\text{W m}^{-2} \text{ sr}^{-1} \mu^{-1}$
$p_a(\theta_s, \theta_v, \Delta\phi) = P_a(\lambda, \gamma^-) + [\rho_F(\theta_s) + \rho_F(\theta_v)] P_a(\lambda, \gamma^+)$		
$P_a(\lambda, \gamma \pm)$	Aerosol phase function, where $\gamma \pm$ is the scattering angle sr^{-1} With $\cos(\gamma \pm) = \pm \cos(\theta_s) \cos(\theta_v) - \sin(\theta_s) \sin(\theta_v) \cos(\Delta\phi)$	
$Q(\lambda, \theta_s, \theta', \Delta\phi)$	Q factor (i.e., E_u/L_u , where E_u is the upwelling irradiance sr just below the surface and L_u the upwelling radiance at the same depth.	
$R(\lambda, \theta_s)$	Reflectance just below sea surface, i.e., the ratio of the Upwelling to downwelling irradiances just below the surface.	dimensionless
$\Re(\theta')$	Geometrical factor, accounting for all refraction and reflection effects at the air-sea interface (Morel and Gentili 1996)	dimensionless
$\Re(\theta') = \left[\frac{(1 - \bar{\rho})}{(1 - \bar{r} R)} \frac{(1 - \rho_F(\theta'))}{n^2} \right]$		
where n is the refractive index of water $\rho_F(\theta)$ is the Fresnel reflection coefficient for incident angle θ		dimensionless
$\bar{\rho}$ is the mean reflection coefficient for the downwelling irradiance at the sea surface		dimensionless
		dimensionless

	\bar{r} is the average reflection for upwelling irradiance at the water-air interface	
ρ	Directional reflectance	dimensionless
	$\rho = \pi L / F_0 \mu_s$	dimensionless
ρ_{ef}	Foam reflectance	dimensionless
$\tau_a(\lambda)$	Aerosol optical thickness	dimensionless
$\tau_r(\lambda)$	Rayleigh optical thickness	dimensionless
$\tau_{oz}(\lambda)$	Optical thickness due to ozone absorption	dimensionless
$t_s(\lambda, \theta_s)$	Irradiance transmittance for a sun zenith angle θ_s and wavelength λ	
	$t_s(\lambda, \theta_s) = E_d(0^+)/\mu_0(F_0)$	dimensionless
$t_d(\lambda, \theta)$	Diffuse transmittance of the atmosphere for angle θ and wavelength λ	dimensionless

Parameters related to primary production:

α^B	Initial slope of the P^B versus E curve	$gC \text{ gChl}^{-1} (\text{mol quanta m}^{-2})^{-1}$
β	Parameter describing the rate of photo-inhibition of primary production	
E_k	Irradiance above which photosynthesis enters the light-independent regime (defined in terms of PAR)	$W \text{ m}^{-2}$
PAR	Photosynthetically available radiation	$W \text{ m}^{-2}$
PUR	Photosynthetically usable radiation	$W \text{ m}^{-2}$
KPUR	Normalizing value of PUR above which photosynthesis enters the light-independent regime (by analogy to E_k).	$W \text{ m}^{-2}$
P	Primary production	$gC \text{ m}^{-2} \text{ s}^{-1}$
P^B_{max}	Maximum rate of photosynthesis per unit biomass	$gC \text{ g(Chl)}^{-1} \text{ h}^{-1}$
P^B_{opt}	Maximum carbon fixation rate within a water column	$gC \text{ g(Chl)}^{-1} \text{ h}^{-1}$
Ψ^*	Cross-section of photosynthesis per unit areal chlorophyll	$m^2 \text{ g(Chl)}^{-1}$

References

- André, J. M. 1992. Ocean color remote-sensing and the subsurface vertical structure of phytoplankton pigments. *Deep-Sea Res.* 39:763–779.
- André, J. M. and A. Morel. 1989. Simulated effects of barometric pressure and ozone content upon the estimate of marine phytoplankton from space. *J. Geophys. Res.* 94:1029–1037.
- . 1991. Atmospheric corrections and interpretation of marine radiances in CZCS imagery, revisited. *Oceanol. Acta* 14:3–22.
- Andreae, M. O. 1996. Raising dust in the greenhouse. *Nature* 380:389–390.
- Antoine, D. and A. Morel. 1996. Oceanic primary production: I. Adaptation of a spectral light-photosynthesis model in view of application to satellite chlorophyll observations. *Global Biogeochemical Cycles* 10:43–55.
- . 1998. Relative importance of multiple scattering by air molecules and aerosols in forming the atmospheric path radiance in the visible and near infrared parts of the spectrum. *Appl. Opt.* 37:2245–2259.
- . 1999. A multiple scattering algorithm for atmospheric correction of remotely-sensed ocean color (MERIS instrument): Principle and implementation for atmospheres carrying various aerosols including absorbing ones. *Int. J. Remote Sensing* 20, no. 9:1875–1916.
- . 2002. Small critters - Big effects. *Science* 296:1980–1982.
- Antoine, D., J. M. André, and A. Morel. 1996. Oceanic primary production: II. Estimation at global scale from satellite (Coastal Zone Color Scanner) chlorophyll. *Global Biogeochemical Cycles* 10:57–69.
- Antoine, D., A. Morel, and J. M. André. 1995. Algal pigment distribution and primary production in the Eastern Mediterranean as derived from Coastal Zone Color Scanner observations. *J. Geophys. Res.* 100:16193–16209.
- Antoine, D., A. Morel, H. R. Gordon, V. F. Banzon, and R. H. Evans. 2005. Bridging ocean color observations of the 1980's and 2000's in search of long-term trends. *J. Geophys. Res.* 110, C06009, doi:10.1029/2004JC002620.
- Babin, M., A. Morel, and B. Gentili. 1996. Remote sensing of surface sun-induced chlorophyll fluorescence: Consequences of natural variations in the optical characteristics of phytoplankton and the quantum yield of chlorophyll a fluorescence. *Int. J. Rem. Sens.* 17:2417–2448.
- Balch, W. M., M. R. Abbott, and R. W. Eppley. 1989a. Remote sensing of primary production. I – A comparison of empirical and semi-analytical algorithms. *Deep-Sea Res.* 36:1201–1217.

- Balch, W. M., R. W. Eppley, and M. R. Abbott. 1989b. Remote sensing of primary production. II – A semi-analytical algorithm based on pigments, temperature and light. *Deep-Sea Res.* 36:281–295.
- Balch, W., R. Evans, J. Brown, G. Feldman, C. McClain, and W. Esaias. 1992. The remote sensing of ocean primary productivity: Use of a new data compilation to test satellite algorithms. *J. Geophys. Res.* 97:2279–2293.
- Behrenfeld, M. J. and P. G. Falkowski. 1997a. A consumer's guide to phytoplankton primary production models. *Limnol. Oceanogr.* 42:1479–1491.
- . 1997b. Photosynthetic rates derived from satellite-based chlorophyll concentration. *Limnol. Oceanogr.* 42:1–20.
- Behrenfeld, M. J., E. Marañón, D. A. Siegel, and S. B. Hooker. 2002. Photoacclimation and nutrient based model of light-saturated photosynthesis for quantifying oceanic primary production. *Marine Ecology Progress Series* 228:103–117.
- Behrenfeld, M. J., O. Prasil, M. Babin, and F. Bruylants. 2004. In search of a physiological basis for covariations in light-limited and light-saturated photosynthesis. *J. Phycol.* 40:4–25.
- Behrenfeld, M. J., E. Boss, D. A. Siegel, and D. M. Shea. 2005. Carbon-based ocean productivity and phytoplankton physiology from space. *Global Biogeochemical Cycles* 19: GB1006, doi:10.1029/2004GB002299.
- Behrenfeld, M. J., J. T. Randerson, C. R. McClain, G. C. Feldman, S. O. Los, C. J. Tucker, P. G. Falkowski, C. R. Field, C. B. Frouin, W. E. Esaias, D. D. Kolber, and N. H. Pollack. 2001. Biospheric primary production during an ENSO transition. *Science* 291:2594–2597.
- Bricaud, A. and A. Morel. 1986. Light attenuation and scattering by phytoplanktonic cells: A theoretical modeling. *Appl. Opt.* 25:571–580.
- . 1987. Atmospheric corrections and interpretation of marine radiances in CZCS imagery: Use of a reflectance model. *Oceanol. Acta SP*, 33–50.
- Bricaud, A., E. Bosc, and D. Antoine. 2002. Algal biomass and sea surface temperature in the Mediterranean Basin: Intercomparison of data from various satellite sensors, and implications for primary production estimates. *Rem. Sens. of Env.* 81, no. 2-3:163–178.
- Bricaud, A., A. Morel, and L. Prieur. 1981. Absorption by dissolved organic matter of the sea (yellow substance) in the U.V. and visible domains. *Limnol. Oceanogr.* 26:43–53.
- Bricaud, A., M. Babin, A. Morel, and H. Claustre. 1995. Variability in the chlorophyll-specific absorption coefficients of natural phytoplankton: Analysis and parameterization. *J. Geophys. Res.* 100:13321–13332.

- Bricaud, A., A. Morel, M. Babin, K. Allali, and H. Claustre. 1998. Variations of light absorption by suspended particles with chlorophyll a concentration in oceanic (Case 1) waters: Analysis and implications for bio-optical models. *J. Geophys. Res.* 103:31033–31044.
- Buiteveld, H., J.H.M. Hakvoort, and M. Donze. 1994. The optical properties of pure water. Pages 174–183 in *Ocean Optics XII*. Edited by J. S. Jaffe, SPIE Proc. 2258.
- Campbell, J. W. 1995. The lognormal distribution as a model for bio-optical variability in the sea. *J. Geophys. Res.* 100:12237–13254.
- Campbell, J., D. Antoine, R. Armstrong, K. Arrigo, W. Balch, R. Barber, M. Behrenfeld, R. Bidigare, J. Bishop, M.-E. Carr, W. Esaias, P. Falkowski, N. Hoepffner, R. Iverson, D. Kiefer, S. Lohrenz, J. Marra, A. Morel, J. Ryan, V. Vedernikov, K. Waters, C. Yentsch, and J. Yoder. 2002. Comparison of algorithms for estimating ocean primary production from surface chlorophyll, temperature and irradiance. *Global Biogeochemical Cycles* 16, no. 3, 10.10129, 2001, GB001444.
- Carr, M.-E., M.A.M. Friedrichs, M. Schmeltz, M. N. Ait , D. Antoine, K. R. Arrigo, I. Asanuma, O. Aumont, R. Barber, M. Behrenfeld, R. Bidigare, E. Buitenhuis, J. Campbell, A. Ciotti, H. Dierssen, M. Dowell, J. Dunne, W. Esaias, B. Gentili, S. Groom, N. Hoepffner, J. Hisisaka, T. Kameda, C. LeQu  , S. Lohrenz, J. Marra, F. M  lin, K. Moore, A. Morel, T. Reddy, J. Ryan, M. Scardi, T. Smyth, K. Turpie, G. Tilstone, K. Waters, and Y. Yamanaka. 2005. A comparison of global estimates of marine primary production from ocean color. *Deep-Sea Research*, in press.
- Chavez, F. P., P. G. Strutton, G. E. Friederich, R. A. Feely, G. A. Feldman, D. Foley, and M. J. McPhaden. 1999. Biological and chemical response of the equatorial Pacific Ocean to the 1997 and 1998 El Ni  o. *Science* 286: 2126–2131.
- Chr  tiennot-Dinet, M. J. 1987. *Atlas du Phytoplancton Marin*. Vol. 3, edited by A. Sournia. Paris: CNRS.
- Clark, D. K. 1981. Phytoplankton algorithms for the Nimbus 7 CZCS. Pages 227–238 in *Oceanography from Space*. Edited by J.F.R. Gower. New York: Plenum Press.
- Clarke, G. L., G. C. Ewing, and C. J. Lorenzen. 1970. Spectra of backscattered light from the sea obtained from aircraft as a measure of chlorophyll concentration. *Science* 167:1119–1121.
- Claustre, H., A. Morel, M. Babin, C. Cailliau, D. Marie, J.-C. Marty, and D. Vaulot. 1999. Variability in particle attenuation and stimulated fluorescence in the tropical and equatorial Pacific: Scales, patterns and some biogeochemical implications. *J. Geophys. Res.* 104:3401–3422.
- Cox, C. and W. Munk. 1954. Statistics of the sea surface derived from sun glitter. *J. Mar. Res.* 13:198–227.
- Cullen, J. J., X. Yang, and H. L. MacIntyre. 1992. Nutrient limitation of marine photosynthesis. Pages 69–88 in *Primary Productivity and Biogeochemical Cycles in the Sea*. Edited by P. G. Falkowski and A. D. Woodhead. New York: Plenum Press.

- Deschamps, P. Y., M. Herman, and D. Tanré. 1983. Modeling of the atmospheric effects and its application to the remote sensing of ocean color. *Applied Optics* 22:3751–3758.
- Deschamps, P. Y., F. M. Bréon, M. Leroy, A. Podaire, A. Bricaud, J. C. Buriez, and G. Sèze. 1994. The POLDER mission: Instrument characteristics and scientific objectives. *IEEE Transactions in Geosciences and Remote Sensing* 32:598–615.
- Deuser, W. G. and E. H. Ross. 1980. Seasonal change in the flux of organic carbon to the deep Sargasso Sea. *Nature* 283:364–365.
- Doerffer, R. and J. Fischer. 1994. Concentrations of chlorophyll, suspended matter, and gelbstoff in case II waters derived from satellite coastal zone color scanner data with inverse modeling methods. *J. Geophys. Res.* 99: 7457–7466.
- Donaghay, P. L., P. S. Liss, R. A. Duce, D. R. Kester, A. K. Hanson, T. Villareal, N. W. Tindale, and D. J. Gifford. 1991. The role of episodic atmospheric nutrient inputs in the chemical and biological dynamics of oceanic ecosystems. *Oceanogr.* 4:62–70.
- Duce, R. A., P. S. Liss, J. T. Merrill, E. L. Atlas, P. Buat-Ménard, B. B. Hicks, J. M. Miller, J. M. Prospero, R. Arimoto, T. M. Church, W. Ellis, J. N. Galloway, L. Hansen, T. D. Jickells, A. H. Knap, K. H. Reinhardt, B. Schneider, A. Soudine, J. J. Tokos, S. Tsunogai, R. Wollast, and M. Zhou. 1991. The atmospheric input of trace species to the world ocean. *Global Biogeochem. Cycles* 5:193–259.
- Dugdale, R. C. and J. J. Goering. 1967. Uptake of new and regenerated forms of nitrogen in primary productivity. *Limnol. Oceanogr.* 12:196–206.
- Dugdale, R. C., A. Morel, A. Bricaud, and F. P. Wilkerson. 1989. Modeling new production in upwelling centers: A case study of modeling new production from remotely sensed temperature and color. *J. Geophys. Res.* 94: 18119–18132.
- Duntley, S. Q. 1963. Light in the sea. *J. Opt. Soc. Am.* 53:214–233.
- Eppley, R. W. and B. J. Peterson. 1979. Particulate organic matter flux and planktonic new production in the deep ocean. *Nature* 282:677–680.
- Evans, R. H. and H. R. Gordon. 1994. Coastal zone color scanner “system calibration”: A retrospective examination. *J. Geophys. Res.* 99:7293–7307.
- Falkowski, P. G. and J. Raven. 1997. *Aquatic Photosynthesis*. Oxford: Blackwell.
- Falkowski, P. G. and A. D. Woodhead, eds. 1992. Primary productivity and biogeochemical cycles in the sea. *Environmental Science Research*, vol. 43. New York: Plenum Press.
- Falkowski, P. G., R. Barber, and V. Smetacek. 1998. Biogeochemical controls and feedbacks on ocean primary production. *Science* 281:200–206.
- Feldman, G. C., N. Kuring, C. Ng, W. Esaias, C. McClain, J. Elrod, N. Maynard, D. Endres, R. Evans, J. Brown, S. Walsh, M. Carle, and G. Podesta. 1989. Ocean color: Availability of the global data set. *EOS* 70:634.

- Field, C. B., M. J. Behrenfeld, J. T. Randerson, and P. G. Falkowski. 1998. Primary production of the biosphere: Integrating terrestrial and oceanic components. *Science* 281:237–240.
- Fraser, R. S., S. Mattoo, E. Yeh, and C. R. McClain. 1997. Algorithm for atmospheric and glint corrections of satellite measurements of ocean pigment. *J. Geophys. Res.* 102:17107–17118.
- Frouin, R., B. A. Franz, and P. J. Werdell. 2003. The SeaWiFS PAR product. In *Algorithm Updates for the Fourth SeaWiFS Data Reprocessing*, NASA Tech. Memo. 2003-206892, vol. 22, edited by S. B. Hooker and E. R. Firestone. Greenbelt, Md: NASA Goddard Space Flight Center.
- Frouin R., M. Schwindling, and P. Y. Deschamps. 1996. Spectral reflectance of sea foam in the visible and near-infrared: In-situ measurements and remote sensing implications. *J. Geophys. Res.* 101:14361–14371.
- Geider, R. J. and H. L. MacIntyre. 2002. Physiology and biochemistry of photosynthesis and algal carbon acquisition. Pages 44–77 in *Phytoplankton Productivity: Carbon Assimilation in Marine and Freshwater Ecosystems*. Edited by P. J. Williams, D. N. Thomas, and C. S. Reynolds. Oxford: Blackwell.
- Gordon, H. R. 1978. Removal of atmospheric effects from satellite imagery of the oceans. *Appl. Opt.* 17:1631–1636.
- . 1979. Diffuse reflectance of the ocean: The theory of its augmentation by chlorophyll a fluorescence at 685 nm. *Appl. Opt.* 18:1161–1166.
- . 1984. Some studies of atmospheric optical variability in relation to CZCS atmospheric correction. NOAA/NESDIS, Contract No. NA-79-SC-00714.
- . 1997. Atmospheric correction of ocean color imagery in the Earth observing system era. *J. Geophys. Res.* 102:17081–17106.
- Gordon, H. R. and D. K. Clark. 1981. Clear water radiances for atmospheric correction of coastal zone color scanner imagery. *Appl. Opt.* 20:4175–4180.
- Gordon, H. R. and M. M. Jacobs. 1977. Albedo of the ocean-atmosphere system: Influence of sea foam. *Appl. Opt.* 16:2257–2260.
- Gordon, H. R. and W. R. McCluney. 1975. Estimation of the depth of sunlight penetration in the sea for remote sensing. *Appl. Opt.* 14:413–416.
- Gordon, H. R. and A. Morel. 1983. Remote assessment of ocean color for interpretation of satellite visible imagery. Edited by R. T. Barber, C.N.K. Mooers, M. J. Bowman, and B. Zeitzschel. Lecture notes on coastal and estuarine studies, 4.
- Gordon, H. R. and M. Wang. 1992a. Surface-roughness considerations for atmospheric correction of ocean color sensors. I: The rayleigh-scattering component. *Appl. Opt.* 31:4247–4260.

- _____. 1992b. Surface-roughness considerations for atmospheric correction of ocean color sensors. II: Error in the retrieved water-leaving radiance. *Appl. Opt.* 31:4261–4267.
- _____. 1994. Retrieval of water-leaving radiance and aerosol optical thickness over the oceans with SeaWiFS: A preliminary algorithm. *Appl. Opt.* 33:443–452.
- Gordon, H. R., J. W. Brown, and R. H. Evans. 1988a. Exact Rayleigh scattering calculations for use with the Nimbus-7 coastal zone color scanner. *Appl. Opt.* 27:862–871.
- Gordon, H. R., O. B. Brown, R. H. Evans, J. W. Brown, R. C. Smith, K. C. Baker, and D. K. Clark. 1988b. A semi-analytical radiance model of ocean color. *J. Geophys. Res.* 93:10909–10924.
- Gordon, H. R., D. K. Clark, J. L. Mueller, and W. A. Hovis. 1980. Phytoplankton pigments from the Nimbus-7 coastal zone color scanner: Comparisons with surface measurements. *Science* 210:63–66.
- Gower, J.F.R., R. Doerffer, and G. A. Borstad. 1999. Interpretation of the 685 nm peak in water-leaving radiance spectra in terms of fluorescence, absorption and scattering, and its observation by MERIS. *Int'l. J. Remote Sens.* 20, no. 9:1771–1786.
- Gregg, W. W. and K. L. Carder. 1990. A simple spectral solar irradiance model for cloudless maritime atmospheres. *Limnol. Oceanogr.* 35:1657–1675.
- Gregg, W. W. and M. E. Conkright. 2002. Decadal changes in global ocean chlorophyll. *Geophys. Res. Lett.* 29, 10.10129/2002GL014689.
- Gregg, W. W., M. E. Conkright, P. Ginoux, J. E. O'Reilly, and N. W. Casey. 2003. Ocean primary production and climate: Global decadal changes. *Geophys. Res. Lett.* 30, no. 15:1809, 10.1029/2003GL016889 09.
- Gross, L., S. Thiria, R. Frouin, and B. G. Mitchell. 2000. Artificial neural networks for modeling the transfer function between marine reflectance and phytoplankton pigment concentration. *J. Geophys. Res.* 105, C2:3483–3495.
- Hahn, C. J., S. G. Warren, J. London, and R. M. Chervin. 1987. Climatological data for clouds over the globe from surface observations. *NDP 026*, Rep. Carbon Dioxide Inf. Cent., Oak Ridge, Tenn.
- Hansen, J., R. Ruedy, J. Glascoe, and M. Sato. 1999. GISS analysis of surface temperature change. *J. Geophys. Res.* 104:30997–31022.
- Helbling, E. W., V. Villafane, M. Ferrario, and O. Holm-Hansen. 1992. Impact of natural ultraviolet radiation on rates of photosynthesis and on specific marine phytoplankton species. *Mar. Ecol. Prog. Ser.* 80:89–100.
- Honjo, S. 1980. Material fluxes and modes of sedimentation in the mesopelagic and bathypelagic zones. *J. Mar. Res.* 38:53–97.

- Hooker, S. B., W. E. Esaias, G. C. Feldman, W. W. Gregg, and C. R. McClain. 1992. *SeaWiFS Technical Report Series: Vol. 1, An Overview of SeaWiFS and Ocean Color*. NASA Tech. Memo. 104566. Greenbelt, Md.: NASA Greenbelt Space Flight Center.
- Hovis, W. A., D. K. Clark, F. Anderson, R. W. Austin, W. H. Wilson, E. T. Baker, D. Ball, H. R. Gordon, J. L. Mueller, S. Z. El Sayed, B. Sturm, R. C. Wrigley, and C. S. Yentsch. 1980. Nimbus-7 coastal zone color scanner: System description and initial imagery. *Science* 210:60–63.
- Hulbert, E. O. 1945. Optics of distilled and natural waters. *J. Opt. Soc. Am.* 35:698–705.
- IOCCG. 1999. Status and plans for satellite ocean-color missions: Considerations for complementary missions. Edited by J. A. Yoder. *Reports of the International Ocean Color Coordinating Group*, No. 2, IOCCG, Dartmouth, Canada.
- _____. 2000. Remote sensing of ocean color in coastal and other optically-complex waters. Edited by S. Sathyendranath. *Reports of the International Ocean Color Coordinating Group*, No. 3, IOCCG, Dartmouth, Canada.
- _____. 2004. Guide to the creation and use of ocean-colour, level-3, binned data products. Edited by D. Antoine. *Reports of the International Ocean-Colour Coordinating Group*, No. 4, IOCCG, Dartmouth, Canada.
- IPCC (Intergovernmental Panel on Climate Change). 2001. *Climate Change 2001: The Scientific Basis*. Edited by J. T. Houghton, Y. Ding, D. J. Griggs, M. Noguer, P. J. Van Der Linden, and D. Xiaosu. New York: Cambridge Univ. Press.
- Jerlov, N. G. 1961. Optical measurements in the eastern North Atlantic. *Medd. Oceanogr. Inst. Göteborg* 38, no. 11: 4–40.
- Keiner, L. E. and C. W. Brown. 1999. Estimating oceanic chlorophyll concentrations with neural networks. *Int. J. Remote Sensing* 20:189–194.
- Koblenz-Mishke, O. I., V. V. Volkovinsky, and J. G. Kabanova. 1970. Plank-ton primary production of the world ocean. Pages 183–193 in *Scientific Exploration of the South Pacific*, edited by W. Wooster. Washington, D.C.: Nat. Acad. Sci.
- Koepke, P. 1984. Effective reflectance of whitecaps. *Appl. Opt.* 23:1816–1824.
- Kozlianinov, M. V. 1957. Nouvel instrument pour la mesure des propriétés optiques des eaux de mer. *Trud. Inst. Okeanol. Akad. Nauk. SSSR* 25:135–142.
- Levitus, S. 1982. Climatological atlas of the world ocean. *NOAA Prof. Paper 13*. Washington, D.C.: U.S. Govt. Print. Off.
- Loisel, H. 1999. Contribution à l'étude des propriétés bio-optiques et du transfert radiatif dans l'océan: Applications. Thèse de Doctorat de l'Université Pierre et Marie Curie.
- Loisel, H. and A. Morel. 1998. Light scattering and chlorophyll concentration in case 1 waters: A reexamination. *Limnol. Oceanogr.* 43:847–858.

- Longhurst, A. R. 1995. *Ecological Geography of the Sea*. March 2001, ISBN 0124555594. San Diego, Calif.: Academic Press.
- Longhurst, A., S. Sathyendranath, T. Platt, and C. Caverhill. 1995. An estimate of global primary production in the ocean from satellite radiometer data. *J. Plankton Res.* 17:1245–1271.
- Martin, J. H., K. H. Coale, K. S. Johnson, S. E. Fitzwater, et al. 1994. Testing the iron hypothesis in ecosystems of the equatorial Pacific Ocean. *Nature* 371:123–129.
- McPeters, R. D. et al. 1996. Nimbus-7 Total Ozone Mapping Spectrometer (TOMS) data products user's guide. *NASA Reference Publication 1384*. Washington, D.C.: National Aeronautics and Space Administration.
- McPhaden, M. J. 1999. Genesis and evolution of the 1997–98 El Niño. *Science* 283:950–954.
- Mobley, C. D. 1994. *Light and Water: Radiative Transfer in Natural Waters*. London: Academic Press.
- Monahan, E. C. and I. O'Muircheartaigh. 1980. Optimal power-law description of oceanic whitecap dependence on wind speed. *J. Phys. Oceanogr.* 10:2094.
- Moore, G.F.M., J. Aiken, and S. J. Lavender. 1999. The atmospheric correction of water colour and the quantitative retrieval of suspended particulate matter in Case II waters: Application to MERIS. *Int. J. Rem. Sens.* 20, no. 9:1713–1733.
- Morel, A. 1966. Etude expérimentale de la diffusion de la lumière par l'eau, les solutions de chlorure de sodium, et l'eau de mer optiquement pures. *J. Chim. Phys.* 10:1359–1366.
- _____. 1973. Diffusion de la lumière par les eaux de mer, résultats expérimentaux et approche théorique. In *Optics of the Sea (Interface and In-water Transmision and Imaging)*. AGARD Lecture Series No. 61, 3.1-1-3.1-76. The original version of this paper was published by the Advisory Group for Aerospace Research and Development, North Atlantic Treaty Organization (RTO/NATO) in Lecture Series, AGARD-LS-61 “Optics of the Sea” in August 1973.
- _____. 1974. Optical properties of pure water and sea water. Pages 1–24 in *Optical Aspects of Oceanography*. Edited by N. G. Jerlov and E. Steemann-Nielsen. London: Academic Press.
- _____. 1978. Available, usable, and stored radiant energy in relation to marine photosynthesis. *Deep Sea Research* 25:673–688.
- _____. 1980. In-water and remote measurements of ocean color. *Boundary-layer Meteorol.* 18:177–201.
- _____. 1988. Optical modeling of the upper ocean in relation to its biogenous matter content (case 1 waters). *J. Geophys. Res.* 93:10749–10768.

- . 1991a. Light and marine photosynthesis: A spectral model with geochemical and climatological implications. *Prog. Oceanogr.* 26:263–306.
- . 1991b. Optics of marine particles and marine optics. Pages 141–188 in *Particle Analysis in Oceanography* NATO ASI series, vol. G27, edited by S. Demers. Berlin: Springer-Verlag.
- Morel, A. and J. M. André. 1991. Pigment distribution and primary production in the western Mediterranean as derived and modeled from coastal zone color scanner observations. *J. Geophys. Res.* 96:12685–12698.
- Morel, A. and D. Antoine. 1994. Heating rate within the upper ocean in relation to its bio optical state. *J. Phys. Oceanogr.* 24:1652–1665.
- Morel, A. and J.-F. Berthon. 1989. Surface pigments, algal biomass profiles, and potential production of the euphotic layer: Relationships reinvestigated in view of remote-sensing applications. *Limnol. Oceanogr.* 34: 1545–1562.
- Morel, A. and A. Bricaud. 1986. Inherent properties of algal cells including picoplankton: Theoretical and experimental results. *Can. Bull. Fish. Aquatic Sci.* 214:521–559.
- Morel, A. and B. Gentili. 1991. Diffuse reflectance of oceanic waters: Its dependence on sun angle as influenced by the molecular scattering contribution. *Appl. Opt.* 30:4427–4438.
- . 1993. Diffuse reflectance of oceanic waters. II. Bidirectional aspects. *Appl. Opt.* 32:6864–6879.
- . 1996. Diffuse reflectance of oceanic waters. III. Implication of the bidirectionality for the remote sensing problem. *Applied Optics* 35:4850–4862.
- Morel, A. and S. Maritorena. 2001. Bio-optical properties of oceanic waters: A reappraisal. *J. Geophys. Res.* 106: 7763–7780.
- Morel, A. and L. Prieur. 1977. Analysis of variations in ocean color. *Limnol. Oceanogr.* 22:709–722.
- Morel, A. and R. C. Smith. 1982. Terminology and units in optical oceanography. *Marine Geodesy* 5:335–349.
- Morel, A., K. J. Voss, and B. Gentili. 1995. Bidirectional reflectances of oceanic waters: A comparison of modeled and measured upward radiance fields. *J. Geophys. Res.* 100:13143–13150.
- Morel, A., D. Antoine, M. Babin, and Y. Dandonneau. 1996. Measured and modeled primary production in the Northeast Atlantic (EUMELI JGOFS program): The impact of natural variations in photosynthetic parameters on model predictive skill. *Deep-Sea Res. I* 43:1273–1304.

- O'Reilly, J. E., S. Maritorena, B. G. Mitchell, D. A. Siegel, K. L. Carder, S. A. Garver, M. Kahru, and C. McClain. 1998. Ocean color chlorophyll algorithms for SeaWiFS. *J. Geophys. Res.* 103:24937–24953.
- Otchakovski, Y. E. 1965. Comaraison des indicatrices mesurées et calculées pour l'eau de mer. *Trud. Inst. Okeanol. Akad. Nauk. SSSR* 77:125–130.
- Pegau, S. and R. Zaneveld. 1993. Temperature dependent absorption of water in the red and near infrared portions of the spectrum. *Limnol. Oceanogr.* 38:188–192.
- Plass, G. N., G. W. Kattawar, and J. A. Quinn Jr. 1975. Radiative transfer in the earth's atmosphere and ocean: Influence of ocean waves. *Appl. Opt.* 14:1924–1936.
- Platt, T. and A. W. Herman. 1983. Remote sensing of phytoplankton in the sea: Surface layer chlorophyll as an estimate of water-column chlorophyll and primary production. *Intl. J. Rem. Sens.* 4:343–351.
- Platt, T. and S. Sathyendranath. 1993. Fundamental issues in measurement of primary production. *Proceedings of Measurement of Primary Production from the Molecular to the Global Scale*, La Rochelle, France, 21–24 April 1992. Edited by W.K.W. Li and S. Maestrini, *Cons. Int. Explor. Mer*, 3–8.
- Platt, T., C. L. Gallegos, and W. G. Harrison. 1980. Photoinhibition of photosynthesis in natural assemblages of marine phytoplankton. *J. Mar. Res.* 38:687–701.
- Platt, T., W. G. Harrison, M. R. Lewis, W.K.W. Li, S. Sathyendranath, R. E. Smith, and A. F. Vezina. 1989. Biological production of the oceans; The case for a consensus. *Mar. Ecol. Prog. Ser.* 52:77–88.
- Pope, R. M. and E. S. Fry. 1997. Absorption spectrum (380–700 nm) of pure water. II. Integrating cavity measurements. *Appl. Opt.* 36:8710–8723.
- Prieur, L. and S. Sathyendranath. 1981. An optical classification of coastal and oceanic waters based on the specific spectral absorption curves of phytoplankton pigments, dissolved organic matter and other particulate materials. *Limnol. Oceanogr.* 26:671–689.
- Purves, W. K., D. Sadava, G. H. Orians, and H. C. Heller. 2003. *Life: The Science of Biology*. 7th ed. Sinauer Associates and W. H. Freeman.
- Rabinowitch, E. and Govindjee. 1969. *Photosynthesis*. New York: John Wiley & Sons.
- Ras, J. 1999. Primary production modelling from ocean color satellite data (SeaWiFS): A practical study on the Mediterranean sea. M.Sc in Oceanography diss., Univ. of Southampton, U.K.
- Rast, M. and J. L. Bézy. 1995. The ESA medium resolution imaging spectrometer (MERIS): Requirements to its mission and performance of its system. Pages 125–132 in RSS95, *Remote Sensing in Action*, Proc. 21st Annual Conf. Remote Sensing Soc., 11–14 September, 1995, University of Southampton, edited by P. J. Curran and Y. C. Robertson. London: Taylor and Francis Pub.

- Reed, R. K. 1977. On estimating insolation over the ocean. *J. Phys. Oceanogr.* 7:482–485.
- Reynolds, R. W. and T. M. Smith. 1995. A high resolution global sea surface temperature climatology. *J. Climate* 8: 1571–1583.
- Ricard, M. 1987. *Atlas du Phytoplancton Marin*. Vol. 2. Edited by A. Sournia. Paris: CNRS.
- Robinson, I. S. 1983. Satellite observations of ocean color. *Philos. Trans. Royal Soc. of London*, Series A, 309:338–347.
- Rossow, W. B. and R. A. Schiffer. 1991. ISCCP cloud data products. *Bull. Amer. Meteor. Soc.* 72:2–20.
- Ryther, J. H. 1969. Photosynthesis and fish production in the sea. *Science* 166:72–76.
- Saitoh, S. 1995. OCTS on ADEOS. Pages 473–480 in *Oceanographic Application of Remote Sensing*. Edited by M. Ikeda and F. W. Dobson. Boca Raton, Fla.: CRC Press.
- Salomonson, V. V., W. L. Barnes, P. W. Maymon, H. E. Montgomery, and X. Ostrow. 1989. MODIS: Advanced facility instrument for studies of the earth as a system. *IEEE Transactions in Geosciences and Remote Sensing* 27:145–152.
- Sasaki, T., N. Okami, and S. Matsumura. 1960. Scattering functions for deep sea water of the Kuroshio. *La Mer* 6, no. 3:165–175.
- Sathyendranath, S. and T. Platt. 1989. Remote sensing of ocean chlorophyll: Consequence of non-uniform pigment profile. *Appl. Optics*. 28:490–495.
- Sathyendranath, S., A. Longhurst, C. M. Caverhill, and T. Platt. 1995. Regionally and seasonally differentiated primary production in the North Atlantic. *Deep-Sea Res.* I 42:1773–1802.
- Sathyendranath, S., T. Platt, E.P.W. Horne, W. G. Harrison, O. Ulloa, R. Outerbridge, and N. Hoepffner. 1991. Estimation of new production in the ocean by compound remote sensing. *Nature* 353:129–133.
- Schiller, H. and R. Doerffer. 1999. Neural network for emulation of an inverse model-operational derivation of case II properties from MERIS data. *Int. J. Remote Sensing* 20, no. 9:1735–1746.
- Schimel, D., I. Enting, M. Heimann, T. Wigley, D. Raynaud, D. Alves, U. Siegenthaler (contributing author list includes Jain, A. K. and others). 1995. CO₂ and the carbon cycle. In *Radiative Forcing of Climate Change: The IPCC WGI 1994 Report*. Cambridge, U.K.: Cambridge University Press.
- Smith, R. C. and K. S. Baker. 1981. Optical properties of the clearest natural waters (200–800nm). *Appl. Opt.* 20: 177–184.

- Smith, R. C., B. B. Prezelin, K. S. Baker, R. R. Bidigare, N. P. Boucher, T. Coley, D. Karentz, S. MacIntyre, H. A. Matlick, D. Menzies, M. Ondrusek, Z. Wan, and K. J. Waters. 1992. Ozone depletion: Ultraviolet radiation and phytoplankton biology in Antarctic waters. *Science* 255:952–959.
- Sogandares, F. M. and E. S. Fry. 1997. Absorption spectrum (340–640 nm) of pure water. I. Photothermal measurements. *Appl. Opt.* 36:8699–8709.
- Steele, J. H. 1962. Environmental control of photosynthesis in the sea. *Limnol. Oceanogr.* 7:137–150.
- Stramski, D. 1994. Gas microbubbles: An assessment of their significance to light scattering in quiescent seas. Page 704–710 in *Ocean Optics XII*. Edited by J. S. Jaffe, Proc. SPIE 2258.
- Sverdrup, H. U. 1953. On conditions for the vernal blooming of phytoplankton. *J. du Conseil* 18:237–295.
- Talling, J. F. 1957. The phytoplankton population as a compound photosynthetic system. *New Phytol.* 56:133–149.
- Turk, D., M. J. McPhaden, A. J. Busalacchi, and M. R. Lewis. 2001. Remotely-sensed biological production in the tropical Pacific during 1992–1999 El Niño and La Niña. *Science* 293:471–474.
- Tyler, J. E. 1961. Scattering properties of distilled and natural waters. *Limnol. Oceanogr.* 6:451–456.
- Van De Hulst, H. C. 1957. Light Scattering by Small Particles. New York: John Wiley & Sons.
- Vermote, E. F., D. Tanré, J. L. Deuzé, M. Herman, and J.J. Morcrette. 1997. *Second Simulation of the Satellite Signal in the Solar Spectrum (6S), Users Guide Version 2.0*. Department of Geography, University of Maryland, Laboratoire d'Optique Atmosphérique, U.S.T.L., Lille, France.
- Viollier, M. 1980. Thèse de Doctorat. Université de Lille, France.
- Wang, M. 1991. Atmospheric correction of the second generation ocean color sensors. Doctor of Philosophy diss., Univ. Miami, Coral Gables, Fla., U.S.
- Webb, W. L., M. Newton, and D. Starr. 1974. Carbon dioxide exchange of *Alnus Rubra*: A mathematical model. *Ecologia* 17:281–291.
- Williams, P.J.L. 1993. On the definition of plankton production terms. Pages 9–19 in *Proceedings of Measurement of Primary Production from the Molecular to the Global Scale*, La Rochelle, France, 21–24 April 1992, edited by W.K.W. Li and S. Maestrini. ICES Marine Science Symp. 197.

- Yan, X.-H., P. P. Niiler, and R. H. Stewart. 1991a. Construction and accuracy analysis of images of the daily-mean mixed-layer depth. *Int. J. Remote Sensing* 12:2573–2584.
- Yan, X.-H., A. Okubo, J. R. Schubel, and D. W. Pritchard. 1991b. An analytical model for remote sensing determination of the mixed layer depth. *Deep-Sea Res.* 38:267–287.
- Yoder, A. Y., C. R. McClain, G. C. Feldman, and W. E. Esaias. 1993. Annual cycles of phytoplankton chlorophyll concentrations in the global ocean: A satellite view. *Global Biogeochem. Cycles* 7:181–193.
- Zhang, X., M. R. Lewis, and B. Johnson. 1998. Influence of bubbles on scattering of light in the ocean. *Appl. Opt.* 37:6525–6536.

